11

Jupiter's Ring-Moon System

Joseph A. Burns
Cornell University

Damon P. Simonelli
Jet Propulsion Laboratory

Mark R. Showalter
Stanford University

Douglas P. Hamilton
University of Maryland

Carolyn C. Porco
Southwest Research Institute

Larry W. Esposito
University of Colorado

Henry Throop
Southwest Research Institute

11.1 INTRODUCTION

Ever since Saturn's rings were sighted in Galileo Galilei's early sky searches, they have been emblematic of the exotic worlds beyond Earth. Now, following discoveries made during a seven-year span a quarter-century ago (Elliot and Kerr 1985), the other giant planets are also recognized to be circumscribed by rings.

Jupiter's diaphanous ring system was unequivocally detected in long-exposure images obtained by Voyager 1 (Owen et al. 1979) after charged-particle absorptions measured by Pioneer 11 five years earlier (Fillius et al. 1975, Acuña and Ness 1976) had hinted at its presence. The Voyager flybys also discovered three small, irregularly shaped satellites—Metis, Adrastea and Thebe in increasing distance from Jupiter—in the same region; they joined the similar, but larger, Amalthea that had first been spied in 1892 by E. E. Barnard. The Cassini imaging system (Porco et al. 2003) looked, without success, for additional small satellites down to about 8 km in radius for an assumed albedo of 0.1 in the region 2.6 to 20 R_J with $i < 1.6°$ and $e < 0.0002$. An initial search (Showalter et al. 2003) of HST images that should have been sensitive to bodies as small as 3-4 km detected none.

An artist's concept of Jupiter's ring-moon system is given in Fig. 11.1, which shows the relative positions of the various components, as well as the intimate relationship between the Jovian ring and its embedded satellites. Adrastea

skirts within the outer stretches of the main ring, while Metis is located ~ 1000 km closer to Jupiter in a region where the ring is depleted. Each of the vertically thick gossamer rings is associated with a moon having a somewhat inclined orbit; the innermost gossamer ring extends towards Jupiter from Amalthea, and exterior gossamer ring is connected similarly with Thebe.

Small moons are always found in the vicinity of planetary rings. Cuzzi et al. 1984 refer to them as "ring-moons," while Burns 1986 calls them "collisional shards." They may act as both sources and sinks for small ring particles (Burns et al. 1984, Burns et al. 2001).

By definition, tenuous rings are very faint, implying that particles are so widely separated that mutual collisions play little role in the evolution of such systems. For reasons that are not well understood, micron-sized grains predominate in faint rings. Such particles become electrically charged in the ambient plasma environment (Grün et al. 1984, Mendis et al. 1984, Horányi 1996, Chapter 10), inducing significant electromagnetic accelerations on micron-sized particles. Small particles are readily destroyed by various processes in the fierce environment near planets, and thus faint rings must be continually replenished if they are long-lived features of the solar system.

For all these reasons, tenuous rings are a distinct class of solar-system structure that engenders considerable interest. In this book, Krüger et al. (Chapter 10) describe the in-
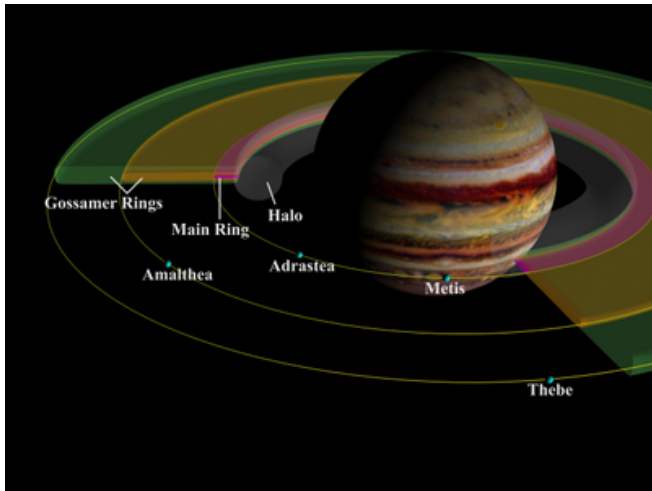
Figure 11.1. A cut-away view of the components of Jupiter's ring System is shown in relation to Jupiter and to the small ring-moons that are described in this chapter. The innermost and thickest ring, shown as a torus, is the *halo* whose outer edge ends at the narrow and flat *main ring*. The main ring is circumscribed by the satellite Adrastea's orbit; it may be partly composed of fine particles knocked off Adrastea, and a somewhat larger moon Metis located about 1000 km closer to the planet. Thebe and Amalthea, satellites that are larger still, supply dust that forms the thicker, washer-like *gossamer rings*; the thicknesses of the gossamer rings are determined by the inclinations of these two satellite orbits. A very faint extension (not shown) of the outer gossamer ring reaches beyond Thebe's orbit. From Ockert-Bell et al. 1999.

situ identification of individual dust grains throughout the jovian magnetosphere by the Galileo spacecraft. The ring-moon system may also provide some clues about the origins of the Galilean moons (Lunine et al., Chapter 2, Hamilton et al. 2001). As the archetype of a dusty ring, Jupiter's has been of more than passing interest to Cassini ring scientists (Porco et al. 2003, Brown et al. 2003). Nevertheless, it is appropriate to note that the Jovian rings contain very little mass, probably much less than the Jovian ring-moons, as well as much less than the other solar-system rings.

After its discovery by Voyager 1 (Smith et al. 1979a), the Jovian ring system was surveyed at visible wavelengths by Voyager 2 later in 1979 (Smith et al. 1979b, see references in Showalter et al. 1987), a handful of times by the Galileo spacecraft between 1996 and 2001 (Ockert-Bell et al. 1999, Burns et al. 2001), and for an extended time by the Cassini spacecraft during its distant flyby in 2000–2001 (Porco et al. 2003). In addition, near-infrared data have been obtained by both Galileo (McMuldroch et al. 2000) and Cassini (Brown et al. 2003). Attempts to detect the ring in occultation and at other wavelengths, albeit with less sensitive instruments, have all been unsuccessful (see references in Burns et al. 1984 and Throop et al. 2003).

Ground-based observations (Nicholson and Matthews 1991, de Pater et al. 1999) have been successful primarily in the near-infrared, where the planet is dim. HST has obtained spectrophotometric data from 1.1-2.05 μm of the rings and Amalthea (Meier et al. 1999). Polarimetric data were taken

serendipitously from HST (J. Goguen, private communication, 1998); polarimetry obtained by Cassini has proven difficult to invert (P. Helfenstein, private communication, 2002; Throop et al. 2003). During the 2002-03 ring-plane crossings Showalter et al. 2003 observed the rings with HST, as did a team at the Keck telescope led by I. de Pater.

A few dust particles were encountered in this region by Pioneer (Elliot and Kerr 1985) and many more were identified by Galileo (Chapter 10). Some of these grains are interplanetary planetary particles; a few of these can even be captured onto retrograde paths (Colwell et al. 1998). The data set obtained during Galileo's sweep past Amalthea in November 2002 contains information on the satellite's mass (Anderson et al. 2002), numerous impacts of gossamer ring particles (Krüger et al. 2003), and unique measurements of magnetospheric properties (S. Bolton, private communication, 2003). Just preliminary analyses of these data were accomplished at the time of this writing.

The Jovian ring system has been previously reviewed by Jewitt 1982, Burns et al. 1984, Burns et al. 2001, Showalter et al. 1987 and Showalter 1989. Surveys of Jovian ring-moons are presented by Thomas and Veverka 1982 and Thomas et al. 1986.

11.2 RING-MOONS

11.2.1 Environment

Jupiter's ring-moon system (Fig. 11.1) encircles the solar system's most massive planet, which is also enveloped by its most energetic magnetosphere. Orbital speeds of constituents are measured in several tens of km/s; velocities for escaping from the entire system from circular orbit are higher by a factor of $\sqrt{2}$, implying that projectiles approaching from infinity move at least that fast. This indicates that mean collision speeds are many tens of km/s whereas head-on impacts occur at as high as 80 km/s, producing substantial ejecta per collision.

Jupiter's inner magnetosphere has been visited only by the Pioneer missions three decades ago (Dessler 1983), by the scantily equipped Galileo probe in 1995 (see Chapters 24 and 27 by Khurana et al. and Bolton et al.), and by the Galileo orbiter itself in late 2002. The few absorptions of high-energy magnetospheric particles observed by Pioneer were deduced to be the "shadows" of Amalthea as well as perhaps of undiscovered rings or moons (Fillius et al. 1975; Acuña and Ness 1976). With the residents of this region now better known, these signatures could be re-visited and more clearly understood today.

Some of the magnetospheric properties in this region may also be inferred from Jupiter's decimetric radiation (de Pater et al. 1997), which suggests the absorption of magnetospheric constituents by ring particles. The very intense radiation environment surrounding Io is believed to decay abruptly as the planet is approached (Dessler 1983 and, especially, updates in this book). Nonetheless the ambient environment throughout this region is fierce, and severely limits the lifetimes of dust motes by sputtering and fragmentation. Among the species present within the inner magnetosphere are likely to be contaminants from Io's volcanoes and surface (ions of S, O, etc.; see Ch. 14 by McEwen et al.).

Dust has been measured throughout the regular satellite system by both the Pioneer (Elliot and Kerr 1985) and the Galileo spacecraft (Chapter 10 by Krüger et al.). Cassini monitored the dust population in Jupiter's neighborhood during its long flyby of the planet. These data indicate that some particles are incoming interplanetary meteoroids which strike the ring-moon system at high speeds; others are ejecta from collisions with the satellites and yet more may be Io's volcanic detritus (Chapter 10 by Krüger et al.).

11.2.2   Orbital Properties and Histories

The orbital properties of the small ring-abutting moons are listed in Table 1, where they are compared to those of the much larger and more distant Galilean satellite Io. The four ring-moons divide naturally into two pairs. Metis and Adrastea, the innermost moons that skirt the outer edge of Jupiter's main ring, have sizes of order 10 km and orbit along almost circular, nearly uninclined paths separated by a scant 1000 km. These orbits are consistent with an origin scenario in which the moonlets condensed from a disk of gas and dust surrounding proto-Jupiter (see Ch. 2 by Lunine et al.). Metis and Adrastea are typical ring-moons, similar to—albeit smaller than—many others residing around each of the giant planets. This duo is notable because of their close orbital spacing and, especially, because of their connection with the main Jovian ring. The proximity of Metis and Adrastea may hint that these objects were born during the breakup of a larger precursor. If this is the case, it may be reasonable to expect smaller, as-yet unnoticed, km- and 100-m-sized fragments in the vicinity.

Thebe and Amalthea, each linked to one of the gossamer rings, are much larger (of order 100 km) than Metis and Adrastea. Their orbits also have larger inclinations i and eccentricities e (Table 1) than the more circular, nearly uninclined paths of the other pair of ring-moons. Measurable inclinations for other inner satellites (e.g., Saturn's Mimas and Tethys, Uranus' Miranda, and Neptune's Naiad) are thought to result from historical or contemporaneous orbital resonances between pairs of satellites. Similarly, Hamilton et al. 2001 argue that both Amalthea and Thebe attained their relatively large inclinations during past resonant interactions with Io; these took place as the latter satellite evolved outward due to tidal interactions with Jupiter. This theory predicts magnitudes of the inclinations that are in close agreement with the observed values (Fig. 11.2). Since the inclinations of the moonlets are intimately tied to the appearance of the Jovian gossamer rings, we reproduce the salient points of this model now.

Tides raised on a planet by a satellite located outside of synchronous orbit (the distance where an object's orbital period matches the planet's spin period, $R_{syn} = 2.24R_J$) cause the moon to evolve outward to a larger orbit. Io is no exception, as suggested by its participation in the Laplace resonance with Europa and Ganymede. As Io drifted outward, some of its resonances swept across the ring region, as well as across the orbits of the moonlets Amalthea and Thebe. The semimajor axes of these ring-moons have changed insignificantly over the age of the Solar System, because the tides that they raise on Jupiter are minuscule. During these slow traverses of Io's resonant locations, the eccentricities and inclinations of the ring-moons were excited. In particu-
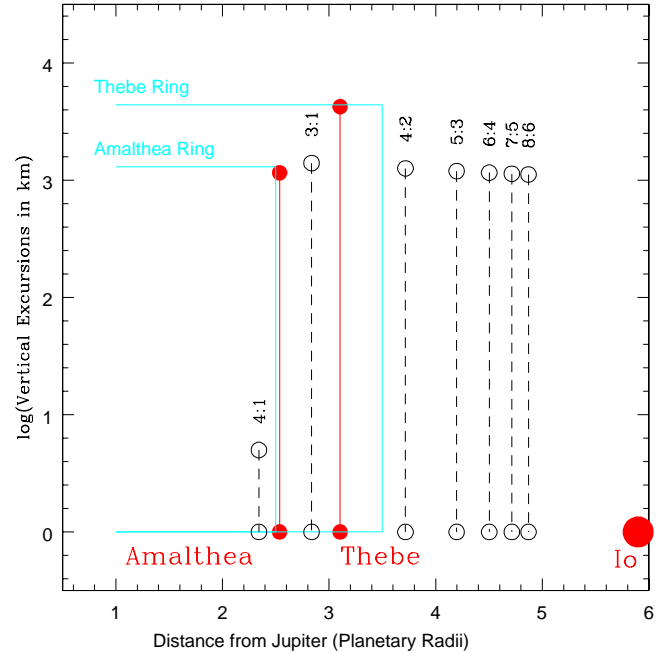
Figure 11.2. The present-day locations (orbital radius, inclination) of the ring-moons Amalthea and Thebe are plotted along with the *current* positions of the primary Io resonances. Solid circles connected by solid lines indicate the present-day vertical excursions of these outermost ring-moons, while open circles linked by dotted lines show the strengths of Io's inclination resonances. As tidal forces draw Io away from Jupiter, its resonances move apace with it and sweep across the orbits of Amalthea and Thebe (i.e., for the resonances to arrive at their locations in this figure, they have moved in from the left). The 3:1 resonance, acting alone, is strong enough to account for Amalthea's inclination, while at least two resonant interactions (the 4:2 and 5:3) must be invoked to explain Thebe's inclination. More discussion is given in the text and by Hamilton et al. 2001.

lar, numerical simulations (Hamilton et al. 2001) show that passage of Io's 3:1 resonance across Amalthea's orbit would be sufficient to generate the current inclination of that satellite (Fig. 11.2). Since further evolution through the 4:2 resonance with Io would have produced an inclination nearly twice what is actually observed, it must not have taken place, thus limiting Io's starting orbital distance to outside about 4.0 R_J. Thebe's larger inclination can be most easily explained as the cumulative result of two, or possibly three, resonant passages. The 4:2 resonance certainly swept across Thebe's orbit, and prior to that the 5:3 and 6:4 may have as well. However, other resonances – including the 7:5 or 8:6 displayed in Fig. 11.2 – did not, for otherwise Thebe's inclination would now be bigger than it actually is. In addition to giving a natural explanation for the enhanced inclinations of Amalthea and Thebe, this resonant-passage model limits

Table 1: Orbital Properties of the Inner Jovian Satellites

Object	Semimajor Axis a in R_J and (km)	Eccentricity e	Inclination i in degrees
Metis	1.792 (128,000)	0.0002	0.06
Adrastea	1.806 (129,000)	0.0015	0.03
Amalthea	2.54 (181,400)	0.0031	0.388
Thebe	3.11 (221,900)	0.0177	1.070
Io	5.91 (421,800)	0.004	0.04

1 $R_J = 71,398$ km. Data compiled from Burns 1986, Burns et al. 1999, Porco et al. 2003 and www.ssd.jpl.nasa.gov.

Table 2: Physical Properties of Jupiter's Ring-Moons

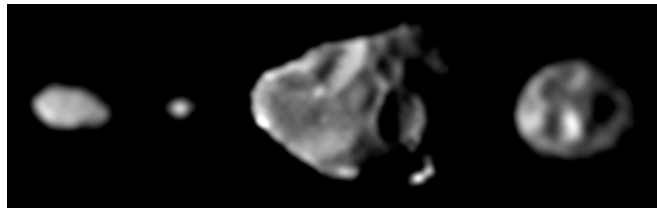| Object	Mean Radius & (Triaxial Radii) (km)	Escape Speed (m/s)	Geometric Albedo
Metis	21.5 (30 x 20 x 17)	0.5-19	0.061
Adrastea	8.2 (10 x 8 x 7)	0-8	-
Amalthea	83.5 (125 x 73 x 64)	30-82	0.090
Thebe	49.3 (58 x 49 x 42)	31-45	0.047

Radii from Thomas et al. 1998; escape speeds from Burns et al. 1999 but see Secs. 11.2.3 and 11.5.1; albedos from Simonelli et al. 2000

Figure 11.3. A first "family portrait" of Jupiter's four small, irregularly shaped inner satellites, taken by Galileo in 1996/1997. The moons are shown in their correct relative sizes, with north approximately up. From left to right, arranged in order of increasing distance from Jupiter, are Metis (longest dimension is approximately 60 km across), Adrastea (20 km across), Amalthea (250 km across), and Thebe (115 km across). The large south-polar crater Gaea is located just below the most prominent, visible circular crater (found in the middle of this Amalthea image); Gaea is "seen" only by its absence and by a segment of its rim, which is the bright patch at 5 o'clock on the limb.

Io's primordial formation distance to between 4.02 and 4.92 R_J (Hamilton et al. 2001).

The orbital eccentricities of Amalthea, and especially Thebe, are also excited during resonant passages. However, tides raised on these satellites by Jupiter dissipate heat inside the bodies, and ultimately damp orbital out-of-roundness (Murray and Dermott 1999). This is exactly the same process that currently powers Io's volcanoes; Io's eccentricity, however, is maintained by the current 2:1 resonant lock with Europa, while the resonant passages that affected Amalthea and Thebe were fleeting. According to this model, the current eccentricities of Amalthea and Thebe, while significant, are lower than they were immediately after the resonant passages.

11.2.3   Satellite Physical Properties

Although the two Voyager spacecraft acquired useful disk-resolved images of Amalthea (Veverka et al. 1981), it was left to the Galileo spacecraft to distinguish Thebe, Adrastea, and Metis as more than pinpoints of light (Thomas et al. 1998). The resulting images (see Fig. 11.3) allow accurate determination of the sizes of all four moons and the shapes of three (see Table 2); in the case of tiny Adrastea, even the best Galileo images are only three to five pixels across, allowing just a gross assessment of shape. Thebe, Amalthea, and Metis all have irregular silhouettes, with the long axes pointing toward Jupiter in the kind of synchronous rotation expected for tidally evolved moons; Amalthea and Metis are especially highly elongated. These complicated shapes—and the fact that Thebe and Amalthea each have several craters whose diameters approach the satellite's mean radius (Table

IV in Thomas et al. 1998)—testify to the severe collisional bombardment experienced by these moons.

Amalthea, the largest of the four moons, was imaged by both Galileo and Voyager, allowing its bulk volume (as represented by the mean radius) to be well constrained. Using the mass detected during Galileo's flyby of Amalthea in November 2002, Anderson et al. 2002 have determined its density to be 1.0 ± 0.5 g-cm^{-3}. This low value suggests that Amalthea is a "rubble pile" (reflecting the moon's intense collisional past), as in the case of Saturn's co-orbital moons (Nicholson et al. 1992). If the material comprising the satellite has an intrinsic density consistent with ordinary silicate rock (roughly 1.5 to 3.5 g-cm^{-3}), as one might expect to be inherited from a circum-Jovian nebula with a hefty Jovian heat source (Pollack and Fanale 1982; see also Lunine et al., Chapter 2), the calculated bulk density implies an internal porosity of 33-70%.

The escape velocities given in Table 2 are the maximum and minimum that were calculated by Burns et al. 1999 for particles thrown at 45° to the surface in the equatorial plane of triaxial ellipsoids having the tabulated shapes and an assumed mass density of 2 g-cm^{-3}. Because of tidal effects and the ring-moons' shapes, these speeds (even the maximum) are much lower than would be the case for isolated spheres of the same size. Amalthea's density is now thought to be only 1 g-cm^{-3} (Anderson et al. 2002), in which case escape speeds drop as low as 1 m/s for parts of its surface (P. Thomas, private communication, 2003). Similar reductions would occur for the other ring-moons if they too are found to be rubble piles.

In terms of globally averaged surface properties, the four small inner moons are all quite dark (see Table 2); geometric albedos are ~ 0.05 to 0.09 in a broad 0.4–1.1 μm filter (Veverka et al. 1981, Thomas et al. 1998, Simonelli et al. 2000). Thebe, Amalthea, and Metis—the trio of satellites large enough to have furnished accurate photometric and spectrophotometric data—all have photometric functions that are similar to those of other small, comparably dark moons, such as Phobos and Deimos (Table II in Simonelli et al. 2000), namely low albedos and considerable

backscattering. Neither Metis or Adrastea have significant opposition surges (Showalter et al. 2003). All the Jovian ring-moons are red, meaning that they brighten at longer visible wavelengths (Veverka et al. 1981, Thomas et al. 1998). Since Voyager days, the color of these moons has been ascribed to contamination from reddish materials ejected by volcanoes on adjacent Io. Contradicting this idea, however, Galileo spectra of Thebe, Amalthea, and Metis reveal that these moons actually get redder the farther they are from Io and the closer they are to Jupiter (Thomas et al. 1998). Furthermore, HST near-infrared data (Meier et al. 1999) suggest that the main Jovian ring—most of which is farther still from Io—is even redder than these moons. Since this as-yet unexplained trend may discredit the contamination hypothesis, future work should improve the modeling of the dynamical histories of volcanic ejecta released by Io and the relative rates at which these contaminants can reach—and modify the colors of—the main Jovian ring and the adjacent small inner satellites (see Chapter 10 by Krüger et al.). Recent HST observations (Showalter et al. 2003) show the ring in backscatter to be less red than the ring-moons and disagree with the conclusion of Meier et al. 1999.

According to Galileo-derived albedo maps of Thebe, Amalthea and Metis, the leading hemispheres of all three satellites are brighter than their respective trailing sides by factors of 1.25 to 1.30 (Simonelli et al. 2000). This consistency from one object to the next suggests that these leading/trailing albedo asymmetries are produced by the same physical process. Thebe and Amalthea are exterior to Jupiter's synchronous orbit R_{syn} (where particles stay above the same Jovian longitude) while Metis at 1.79 R_J lies inside this distance. Thus, this shared physical mechanism is not predominantly bombardment by magnetospheric charged particles because, ignoring small electromagnetic drift velocities, the latter are tied to Jupiter's synchronously rotating magnetic field. Instead, the asymmetry is most likely produced by impacts of macroscopic meteoroids that originated outside the Jovian system (Thomas et al. 1998, Simonelli et al. 2000), because the flux of interplanetary meteoroids preferentially scours the leading sides of these swiftly orbiting moons. Since these meteoroid impacts into the small satellites are believed to also generate the dust that forms Jupiter's rings (see Sec. 11.5.1 below), the leading/trailing asymmetries and the ring-origin models dovetail nicely. What is not clear yet, however, is the precise process by which the enhanced meteoroid flux brightens the leading sides of these moons.

Imaging was not attempted during Galileo's November 2002 very close flyby of Amalthea. However, earlier, in the period from late 1999 to early 2002, long after Galileo had successfully finished its 2-year "prime mission," NASA risked dropping the spacecraft near enough to Jupiter to make six flybys of Io, which necessarily brought Galileo closer than previously to the ring-moons. The resulting images of Thebe, Amalthea, and Metis—the highest-resolution images ever acquired of the small inner Jovian satellites (Figs. 11.4 and 11.5)—not only attest to the large impact craters mentioned earlier, but also disclose, especially in the case of Amalthea, a complex, rough surface of ridges, smaller craters, and albedo splotches. The latter patterns are striking in both their high contrast and their geologic setting. The brightest albedo features on Amalthea are found in,
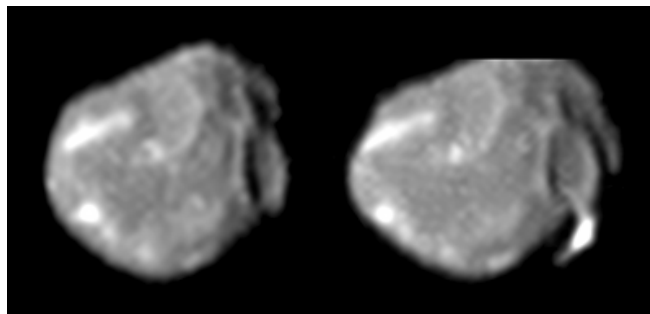
Figure 11.4. Two Galileo images of Amalthea showing similar territory: the anti-Jupiter hemisphere of the satellite (left side of each disk) and leading side of the satellite (right side of each disk) at an image scale of 3.8 to 4.5 km/pixel, making them among the finest-resolution images ever taken of Amalthea. The large impact crater visible in both images near the disk's right-hand edge is about 40 km across; two ridges, tall enough to cast shadows, extend from the shoulders of the crater in a V-shape reminiscent of a "rabbit-ears" television antenna. As visible in Fig. 11.3 (just above the large circular crater), these seem to be the rim of a smaller crater. To the left of these ridges, in the top center of Amalthea's disk, is a second, subdued large impact crater similar in size to the first crater; further left of this second crater is Ida, a linear "streak" of relatively bright material about 50 km long (see text). Other relatively bright patches, e.g., the feature visible only in the right image at 5 o'clock on the limb (see also Fig. 11.3 where this feature appears as an isolated bright island to the lower right of the crater) can be seen elsewhere on Amalthea's disk. In both images, sunlight comes from the left and north is approximately up. Note that in the right image Amalthea's north pole was cut off by the edge of the SSI camera frame.

and along the rims of, the south-polar crater Gaea and the northern-hemisphere crater Pan. Gaea's material in particular is two to three times more reflective than typical Amalthea surface material (Simonelli et al. 2000) and recalls the way that large impacts can create glassy melts or excavate fresh bright material from below an Io-contaminated surface (e.g., Gradie et al. 1980, Gradie et al. 1984).

Other prominent bright features, named Ida and Lyctos, near the pointy, anti-Jupiter "beak" of Amalthea, were seen as round "spots" by Voyager; however, Galileo discerned Ida to be a 50-km-long linear "streak" (Fig. 11.4) that could represent ejecta from a nearby impact crater or might instead merely mark the crest of a local ridge. The latter possibility, if true, mimics a relationship between albedo and topography sometimes present on other small solar-system objects such as Deimos and Gaspra (Thomas et al. 1996, Helfenstein et al. 1994). In these cases, downslope motion of loose debris exposes brighter surfaces at the ridge crest (material that may contain smaller, more transparent particles or otherwise be "fresher" in some way; cf. Gradie et al. 1980). Amalthea's intriguing albedo patterns—combined with the contaminants transported from Io, and the meteoroid impacts that are thought to generate the ring dust—may manifest the presence of a significant regolith on Amalthea, and probably on Thebe as well. On the smaller, lower-gravity Adrastea and Metis, which shed material to the rings more easily (see the Escape Speed column of Ta-
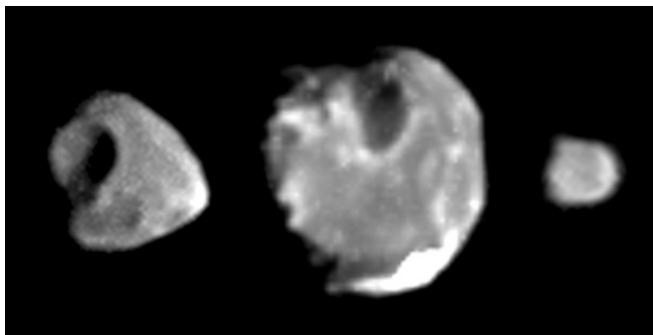
Figure 11.5. These Galileo images of Thebe, Amalthea, and Metis (left to right) are the highest-resolution views yet obtained of these satellites, having image scales of 1.9 km/pixel, 2.4 km/pixel, and 3 km/pixel, respectively. The moons are displayed in their correct relative sizes, with sunlight coming from the right; we are viewing primarily the anti-Jupiter side of each moon, and north is approximately up. The prominent impact crater on Thebe, named Zethus, is about 40 km across. The large white tract near Amalthea's south pole marks the location of the brightest patch of surface material seen on these three moons; it is inside—and on the rim of—the large crater Gaea. This unusual region is greatly overexposed and has "bled" upwards across the camera's CCD; accordingly, the white area is larger than the true bright portion of Amalthea. Note also the "scalloped" or "saw-tooth" shape of Amalthea's terminator (at the left-hand edge of this moon's disk), which indicates that parts of this satellite's surface are very rough, with many small hills and valleys.

ble 2), it is uncertain whether a steady-state regolith with a meaningful thickness exists.

The Voyager images hint that the material at Gaea is greenish compared to the rest of Amalthea (Veverka et al. 1981, Thomas et al. 1998), further emphasizing the possibility of exotic local surface compositions such as impact-produced glasses (e.g., Gradie et al. 1980, Gradie et al. 1984). Galileo, however, was not able to repeat this Gaea observation—and only recorded limited information about how albedo spots on any of these moons differ in color from typical satellite locales (see the color data on three Amalthea and Thebe bright spots in Thomas et al. 1998)—another unhappy consequence of the spacecraft's inoperative high-gain antenna. Color observations of the small inner moons were limited to "on-chip mosaics" where satellite images taken through different filters sit side-by-side on the camera's CCD. Accordingly, these mosaics often have significant charged-particle radiation noise—which also meant that they had to be taken far from Jupiter, when the satellite disks were merely a few pixels across and Gaea only one or two. Better color information about Gaea—and, in fact, improved, higher-SNR color observations for the entire surfaces of the four ring-moons, not only in the visible but in the near-infrared—is needed because it would yield valuable compositional information.

11.3 JUPITER'S RINGS

The Jovian ring, the quintessential dusty planetary ring, was discovered in a single 11-minute exposure by Voyager 1's wide-angle camera (Owen et al. 1979, Smith et al. 1979a). This image was specifically targeted to look for faint ring material during Voyager's crossing of the equatorial plane, and it fortuitously captured the ring's outer edge. Subsequently, Voyager 2 carried out a more extensive imaging sequence (Smith et al. 1979b). The Voyager images were originally interpreted by Jewitt and Danielson 1981 and Jewitt 1982, and then examined more thoroughly by Showalter et al. 1987 (see also Showalter et al. 1985 and Showalter 1989). Recently the Galileo and Cassini spacecraft investigated the ring system in greater detail and from a more diverse set of viewing geometries, respectively. Ockert-Bell et al. 1999 carried out the initial analysis of the Galileo imaging data, supplemented by Burns et al. 1999 and Showalter et al. 2001. Spectral cubes obtained at high phase angles by the Galileo Near-Infrared Mapping Spectrometer (NIMS) covered wavelengths between 1 and 5 μm at high phase (Mc-Muldroch et al. 2000, Brooks et al. 2003). Within the time period of the Galileo tour, de Pater et al. 1999 also acquired images with the 10-m W. M. Keck telescope on Mauna Kea, which rival the Galileo data in their overall sensitivity, although at somewhat coarser spatial resolution and solely in the back-scattered geometry. During Cassini's flyby of Jupiter, the rings and inner satellites were observed at phase angles ranging 0–120°, filling in holes in the phase curves left by previous spacecraft (Porco et al. 2003, Throop et al. 2003). Our knowledge of the Jovian ring system's detailed structure comes almost exclusively from these four data sets.

Other observations provide a few additional details of the ring system's structure and light-scattering properties. Hubble images from NICMOS show the ring in backscatter at 1–2 μm wavelengths (Meier et al. 1999). Cassini's Visual and Infrared Mapping Spectrometer (VIMS), which is more sophisticated than Galileo's NIMS, obtained comparable spectra at 0–120° phase and 1.7–3.5 μm (Brown et al. 2003). Earth-based images, in the methane absorption bands of the near-IR, have also been of value (Nicholson and Matthews 1991). The Hubble Space Telescope and the Keck telescope have mapped out the Jovian ring's phase curve at low elevation angles in the visual and near-IR when the planet went through opposition in winter 2002-03. Galileo's plasma and dust instruments detected signals due to ring-particle impacts during the spacecraft's plunge through the outer gossamer rings (S. Bolton, private communication, 2002, and Krüger et al. 2003).

The Jovian ring system has three components (Fig. 11.1), each described in a separate sub-section below. The main ring, the brightest of these, has Adrastea, a tiny ring-moon, skimming through its outer edge at 1.806 R_J (Jovian radius $R_J = 71,398$ km). Near its inner boundary at about 1.71 R_J (Showalter et al. 1987, Ockert-Bell et al. 1999), the main ring transitions into the vertically extended halo. The halo is radially confined, seeming to fade significantly inward of 1.29 R_J, and vertically extended, rising to a full thickness of $\sim 20,000$ km (about 10°), although the majority of material falls within 1000 km of the ring plane. Two "gossamer" rings that stretch beyond the main ring were discovered in a single Voyager image and surveyed in greater

detail by Galileo, Keck and HST. The orbits of the satellites Amalthea and Thebe circumscribe these thickened, radially smooth bands. Since the ring particles have been shown to have orbital inclinations matching those of their bounding moons, the gossamer rings are likely composed of inward-drifting particles that have been kicked off these satellites by impacting meteoroids (Burns et al. 1999; see Sec. 11.5). By Occam's Razor, the main ring is at least partially derived from the impact debris of Metis and its smaller sibling Adrastea, the small ring-moons described above.

It was initially a surprise when the Jovian ring was found to brighten substantially at high phase angles in the Voyager data. This brightening indicates that the ring contains a large population of micron-sized dust, which diffracts light forward into the range of scattering angles observed (i.e., a few degrees). Burns et al. 1980 first noted that such tiny dust grains cannot survive for long in Jupiter's lethal environs, and so must be replenished continuously from a population of parent bodies, including the known embedded moons. Photometry and spectrophotometry, coupled with dynamical modelling, provide the key to unraveling the relative populations of dust and larger bodies, as well as the origins and dynamical evolution of the entire ring-moon complex.

11.3.1 Main Ring

The main ring –a relatively bright, narrow band, approximately 6,000 km across– is the system's most prominent component (Figs. 11.1 and 11.6). It has a gradual inner boundary but a somewhat more abrupt outer edge, close to Adrastea's orbit. Our understanding of the precise relationship between Adrastea and the ring edge has evolved over the years. Showalter et al. 1987 placed the ring's outer edge at $129, 130 \pm 70$ km, or $1.8086\ R_J$, slightly beyond Adrastea's orbit at 129,000 km (cf. Table 1). However, Ockert-Bell et al. 1999 positioned the outer edge at $128, 940 \pm 73$ km, or $1.8059\ R_J$, suggesting that it is in fact bounded by and shepherded by the tiny moon. Part of the discrepancy is related to the fact that the outer edge, though sharper than the inner, is still rather gradual, with the intensity decaying over a radial span of several hundred km. However, the full explanation became clear when Showalter et al. 2001 subsequently noted a rather surprising trait of the ring—its outer edge location varies with phase angle. Fig. 11.7 shows a pair of profiles of the Jovian ring, obtained from Galileo images at high and low phase angles. In backscattered light, which emphasizes the embedded parent bodies, the ring clearly extends out beyond the orbit of Adrastea, which itself seems to clear a gap. In forward-scattered light, which emphasizes the fine dust present, the ring brightness drops off quickly at Amalthea as Ockert-Bell et al. 1999 described, although some dusty material is found beyond that moon's orbit as well.

Metis, on the other hand, unambiguously resides within a lower-brightness band. Figs. 11.6 and 11.7 show additional ring structure between the two moons, but fine detail interior to the orbit of Metis is absent. The simplest interpretation is that the ring's parent population is concentrated around and between the two moons. Adrastea sweeps clear a gap, whereas Metis defines the population's inner edge. Interior to the orbit of Metis only dust is present, explaining why
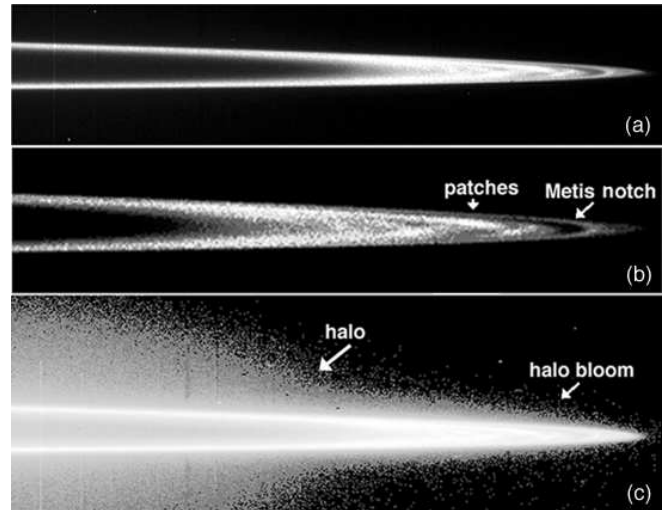
Figure 11.6. A Galileo view (image # 368991900 at a phase angle of 176°) of the Jovian ring's west ansa, showing both the main ring and the halo's outer parts (cf. Fig. 11.1), processed in three different ways to highlight various features. (a) Stretched to differentiate the main ring's diffuse inner periphery versus its much crisper outer boundary. (b) A stretch that emphasizes the patchy nature of the main ring's central region located just interior to a brightness dip associated with Metis's orbit. Features that are bright just above a horizontal line through the ansa tend to become dark just below the line, and vice-versa. (c) By emphasizing fainter structures, the halo's development at the main ring's inner edge is revealed; it appears that the main ring itself is enshrouded in a faint cloud of material, the so-called "halo bloom", above and below. Adapted from Ockert-Bell et al. 1999.

the ring's profile in this region is featureless, and is similar at low and high phase angles.

Adrastea and Metis were implicated by Burns et al. 1999 as the primary sources for the ring's dust, but Fig. 11.7 indicates that this suggestion must be modified. The population of parent bodies, other than the ring-moons, can be estimated from this plot; it has a radially integrated, backscattering intensity (equivalent to the area under the low-phase curve in Fig. 11.7) of $E \simeq 0.4\ m$. The units of the area beneath this curve turn out to be length because the abscissa plots ring radius (given in km) while the ordinate shows the intensity I, measured here via the dimensionless ratio I/F. For the latter quantity πF is the incident solar flux density; by this definition, the I/F of an object in backscatter is equivalent to its geometric albedo. Assuming that the parent bodies have a geometric albedo $p = 0.06$, comparable to that of Metis (see Table 2 above), the total cross-section σ of parent bodies lying in a band of radius r is then

$$\sigma \simeq 2\pi r E/p, \qquad (1)$$

or about 5000 km². For comparison, Metis and Adrastea have cross-sections of 1500 and 200 km², respectively. Thus the moons comprise only one-third of the ring's total target area in source bodies. However, as discussed later in this section, the moons likely contain most of the system's mass. In a sense, the two moons are simply the largest of the embed-
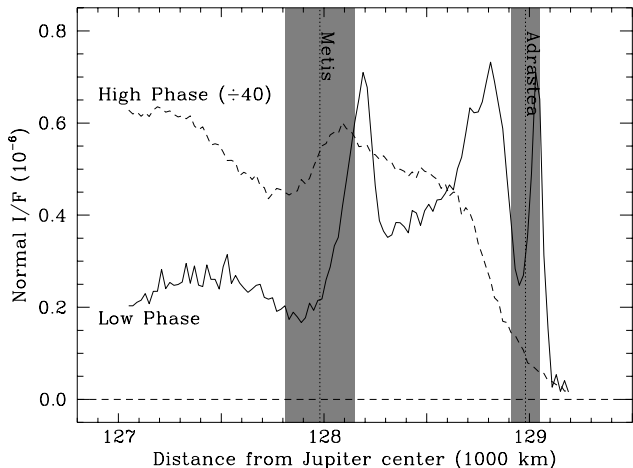
Figure 11.7. A comparison of radial profiles of the main ring's outer region at high and low phase angles, from Galileo images. The low-phase profile shows significant structure between the orbits of Adrastea and Metis, which is not present in the high-phase profile. The former indicates the locations of larger, parent bodies within the system, whereas the latter profile represents the dust. This dust is presumably ejected from the parent bodies and then evolves inward under Poynting-Robertson drag while being pushed about by electromagnetic forces. Vertical lines locate the orbital semimajor axes of Adrastea and Metis; the shaded vertical bands surrounding these orbital positions show the sweeping zones of the satellites (see Eq. 5). Adapted from Showalter et al. 2001.

ded parent bodies. Moreover, they may be the progenitors of the unseen material that provide the area that we have just estimated. Considering the swath of parent bodies to extend over a width $W = 2000$ km, the main ring's optical depth

$$\tau \simeq \sigma/(2\pi r W) = E/(pW) \simeq 3 \times 10^{-6}. \qquad (2)$$

Different values have been measured for the vertical thickness of the main ring. The edge-on discovery image from Voyager 1 places a firm upper limit of 30 km on the ring's full vertical thickness (at half maximum) in backscatter (Smith et al. 1979a, Showalter et al. 1987). In addition, Galileo observed the rings edge-on from a phase angle near $90°$, finding that the full thickness is ~ 100 km, differing somewhat from the backscatter result (Ockert-Bell et al. 1999). Thus, the ring's thickness, like its radial structure, may depend on phase angle. The thinner value could suggest that a collisionally evolved parent population (emphasized in backscatter) is very thin, whereas the dust (somewhat more prominent at intermediate phase angles) has a broader vertical extent owing to electromagnetic scattering. The only thickness determination in forward-scatter is that by Showalter et al. 1987, who placed a crude upper limit of 300 km. This is consistent with the other measurements but does not disallow further thickening with increasing phase. This interpretation is complicated by Porco et al. 2003 and Evans et al. 2003 who find non-zero inclinations for Metis

and Adrastea, corresponding to vertical excursions of ± 60 km and ± 80 km, respectively, which predict a minimum full ring thickness of ~ 150 km.

A number of investigators have photometrically modeled the ring's phase behavior (Figs. 11.8 and 11.9) to infer the size distribution of the dust. All but the latest models consider just Mie scattering. Using Voyager ISS data, Showalter et al. 1987 found that the brightness of the ring's forward-scattered light is well represented by a differential power-law size distribution of the form

$$n(r) = C(r/\mu m)^{-q}, \qquad (3)$$

where $n(r)dr$ is the number of particles between radius r and $r + dr$, q is the so-called power-law index, with larger q implying a steeper size distribution, and C is a normalization constant. Such a representation has the advantages of simplicity and of being common in nature, where q often lies between 2.5 and 3.5. Showalter et al. found $q = 2.5 \pm 0.5$ in the size range between sub-micron and tens of microns, accounting for a total optical depth of $\sim 3 \times 10^{-6}$. The ring's distinctly red hue at these phase angles can be interpreted as resulting from a similar size distribution (Showalter et al. 1987).

Galileo NIMS data at higher phase angles and longer wavelengths were added to the mix by McMuldroch et al. 2000, who found that the newer data were incompatible with the Showalter et al. 1987 model. They preferred a much steeper power law ($q = 3.9 \pm 0.2$) for the smaller particles plus a log-normal distribution centered at a mean radius of 4.5 μm. Brooks et al. 2003 have recently re-analyzed the NIMS data and have included the Galileo SSI and Voyager images as well. Their results match the data of Showalter et al. 1987 better if $q = 2.0 \pm 0.3$ below $r = 15$ μm (Fig. 11.8). For larger sizes, examination of the NIMS results shows that the size distribution steepens to $q = 5.0 \pm 1.5$ in reasonable accord with the analysis of McMuldroch et al. 2000. Brooks et al. believe that all these results can be reconciled with a "broken" power law having $q = 2$ below 15 μm and $q = 5$ for larger sizes. McMuldroch's and Brooks' inferred size distributions are quite similar over the range of sizes sampled by Galileo's infrared device (Fig. 11.8).

After combining Cassini imaging results with the previous data, Porco et al. 2003 have constructed a photometric model for the main ring that incorporates non-spherical dust grains. This was necessary because Mie spheres are artificially subdued in brightness at the intermediate phase angles well-sampled by Cassini (cf. Showalter et al. 1992's similar work on Saturn's F ring). Furthermore, non-spherical particles are more physically plausible, as it is unlikely that dust produced by the erosion of parent bodies will be spherical. This approach achieved a satisfactory overall fit across the available range of phase angles (Fig. 11.9). For example, the observations do not indicate the low-phase brightness surge that is characteristic of Mie-scatterers; however, they are well matched by a non-spherical particle phase-curve (Mishchenko and Travis 1998).

The preferred model of Porco et al. 2003 (see also Throop et al. 2003) is a combination of (i) large parent bodies having a Callisto-like phase function and an albedo of 0.063, like that of Metis, and (ii) non-spherical dust grains 0.01 to 15 μm with a power-law index $q = 2$ which increases to $q = 5$ once $r > 15$ μm. The optical depth of the large
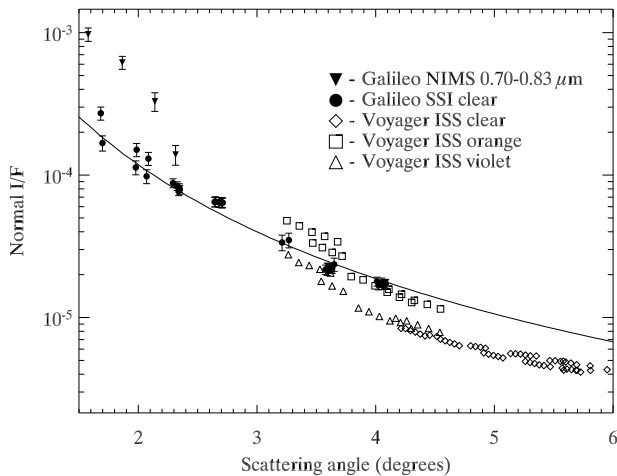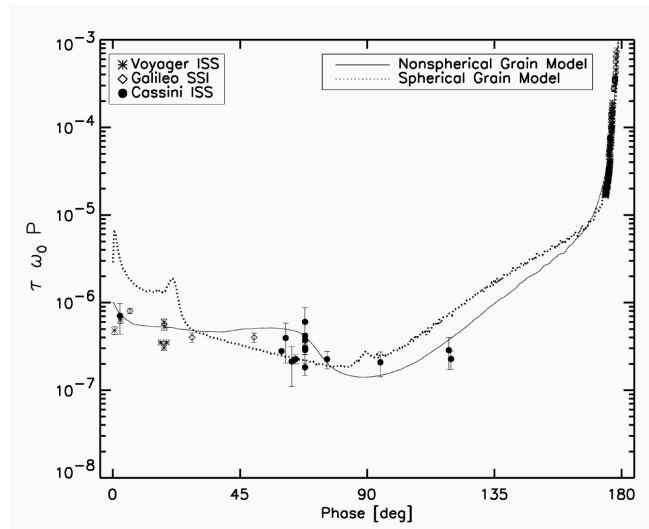
Figure 11.8. Brightness measurements of the main ring at the low scattering angles (diffracted light) that are diagnostic of dust grain sizes. The Galileo data were all derived from images taken through the clear filter, which is a broadband filter with an effective wavelength of 0.6249 μm under solar illumination. Voyager's clear filter has an effective wavelength of 0.5 μm. The orange and violet filters of the Voyager ISS camera pass light centered at 0.61 μm and 0.43 μm, respectively (Showalter et al. 1987). The plotted abscissa is proportional to I/F. The solid line represents a fit to the Galileo SSI observations for an ensemble of particles with a power-law size distribution (Eq. 3) having q = 2; this is consistent with the phase curve derived from the Voyager ISS images. Also plotted for comparison is the average ring brightness seen by NIMS between 0.70 μm and 0.83 μm at four phase angles. The different brightness levels measured within both the Voyager and Galileo data sets at the same scattering angles are primarily caused by the asymmetry discussed in the text. The full phase behavior is shown in the following plot. From Brooks et al. 2003.

Figure 11.9. The phase behavior of the main Jovian ring at visible wavelengths over all phase angles. Values are given in units of I/F as measured normal to the ring plane at the observed phase angle. Cassini observations are plotted along with results from both the Voyager (Showalter et al. 1987) and Galileo imaging experiments (Showalter et al. 2001 and Brooks et al. 2003). Both the best-fitting non-spherical and spherical grain models (as described in the text) are plotted. The forward-scattering results (i.e., the steep right-hand portion of the curve) are seen more clearly in the previous figure, where the abscissa is the scattering angle, or 180°- phase angle. From Porco et al. 2003.

bodies is $\tau_l = (1\text{–}3) \times 10^{-6}$, closely matching the total cross-section derived above based on the ring's radial structure in backscatter (Eq. 2); see also Fig. 4 of Throop et al. 2003. The total optical depth in small particles is $\tau_s = 2 \times 10^{-6}$, again similar to earlier determinations. Further refinements in jovian ring photometric analysis by Throop et al. 2003 include the addition of all available ground-based and spacecraft data sets on the ring (which taken together span phase angles from 0.5–178°, and wavelengths 0.4–4 μm), as well as modeling of the ring's spectrum. They, as in the McMuldroch et al., Brooks et al. and Porco et al. models, indicate that dust area comes predominantly from particles around 15 μm in order to match the NIMS high-phase, near-IR spectrum. It is unclear whether this size is favored because grains are born this way or because evolutionary processes favor this radius.

From the known size distribution of the forward-scattering particles, the total mass producing the diffracted signal can be readily estimated as only $10^{7\text{–}9}$ kg or that contained in a body tens of meters in radius. In such an integration, the largest ($r > 15\mu$m) particles contribute little total mass because of their scarcity in this steep size distri-

bution. However, the true mass of the back-scattering population is unknown without having the size distribution of the very largest members, the parent bodies, that are distinct from the power-law population. The total optical depth of "parent bodies" (see above) is available; however the mass encompassed by these bodies depends on typical sizes (e.g., the 5000 km^2 cross-section estimated above would amount to $\sim 10^{11}$ kg if in cm-sized pebbles, but $\sim 10^{16}$ kg if in 1-km mini-moons). At any rate, the ring's mass is certainly insignificant compared to that of the ring-moons, implying that the moons and their debris amount to almost-infinite suppliers of this ethereal disk. The mass of Jupiter's rings is also much less than those of other ring systems.

The interpretation that the ring's backscatter contains an appreciable signal from parent bodies is supported by the ring's very red color at visible (Showalter et al. 1987) and infrared wavelengths (Throop et al. 2003); the color is similar to that of Adrastea (Meier et al. 1999) and Amalthea (Thomas et al. 1998, Simonelli et al. 2000; however, cf. Showalter et al. 2003). Gradie et al. 1980 proposed that sulfur contamination from Io, combined with impacts by micrometeoroids and magnetospheric particles, act to darken and redden Amalthea's surface; if so, the ring's parent bodies should have been similarly bombarded and colored. That is to say, whatever process acts on the known ring-moons should affect their unseen siblings equally well.

Any photometric analysis of Jupiter's main ring immediately reveals one of its most puzzling features—brightness levels that differ with longitude, apparent most obviously as

distinct brightnesses of the near and far arms. These seem to be a broad longitudinal brightness variation that is not associated with viewing geometry. The property has only been noted at high phase angles, where variations of 10–20% are common (Showalter et al. 1987, Ockert-Bell et al. 1999, Brooks et al. 2003; see the "scatter" at fixed phase angles in Fig. 11.8). The phenomenon has been investigated most thoroughly by Brooks et al. 2003, who maintain that the effect is not associated with any particular longitude in Jupiter's magnetic field, nor any with respect to the Sun nor to the observer. According to the limited available measurements from Galileo, this behavior is more pronounced on the west ansa than the east one, and does not depend strongly on the angular distance from the ansa. The asymmetry seen in the Galileo images is in the opposite sense from that visible in Voyager data. Cassini images did not exhibit any such asymmetry but, owing to low SNR from scattered light, would have only detected $> 50\%$ brightness changes over $10°$-wide swaths in azimuth (Throop et al. 2003). Further analysis of the Cassini data should narrow these limits.

Early speculation by Showalter et al. 1987 suggested that the effect might be a quadrant asymmetry (after the addition of Galileo data, Brooks et al. 2003 argue that this is certainly not the case), reminiscent of a similar phenomenon observed in Saturn's A Ring (Cuzzi et al. 1984, Esposito et al. 1984), where it is considered to be due to clustering in the gravitational wakes of large ring particles. However, since all particles are visible in tenuous rings, any brightness variability cannot be related to changes in the ring geometry. Hence the explanation for variations in an optically thin ring is necessarily quite different from that in Saturn's dense A Ring. Perhaps ring particles are elongated and preferentially aligned, like interstellar dust. Brooks et al. 2003 believe that the variations are best explained by transient clouds of debris released during mutual collisions between parent bodies, similar to Barbara and Esposito 2002's model for the brightness variations in Saturn's F Ring (cf. Showalter 1998).

Another puzzling feature of the main ring is a "patchiness," first reported by Ockert-Bell et al. 1999 (Fig. 11.6b). These patches are $\pm 10\%$ brightness variations in both radius and longitude, occupying the region a few thousand km interior to the orbit of Metis (Figs. 11.6). Radial scales are 500–1000 km. Unfortunately, this phenomenon was observed in only a single sequence of Galileo images, taken at a high phase angle and a small ring-opening angle. Owing to the limited temporal coverage of Galileo images, the time-variability of these structures is undetermined. Because the contrast seems to reverse when crossing the ansa, bright features becoming dark and dark ones becoming bright (Showalter et al. 2001), the most plausible interpretation is that the patches are produced by vertical corrugations in the ring plane (Ockert-Bell et al. 1999). However, no dynamical explanation for such corrugations has been proposed. Alternatively, the variations may indicate a spoke-like phenomenon, transitory debris from recent impacts (Horányi, personal communication, 1999), or perhaps they are merely smaller clumps otherwise similar to the longitudinal variations described above (Brooks et al. 2003).

11.3.2   Halo

The Jovian halo arises near the inner edge of the main ring (Figs. 11.1 and 11.6), and rapidly grows in thickness to 20,000–40,000 km. By studying the way the halo's brightness diminishes upon entering Jupiter's shadow in high-phase Voyager images, Showalter et al. 1987 were able to determine its cross-sectional profile. They found that the halo opens up into a torus, which disappears from view at an inner radius of approximately 100,000 km (1.40 R_J). Fig. 11.10 displays the results of similar processing applied to a pair of Galileo images (Showalter et al. 2001). No vertical asymmetry has been detected; the upper limit to any vertical offset from the equator is ~ 100 km (Showalter et al. 1987).

The large thicknesses generally quoted for the Jovian halo are somewhat misleading, however, because they refer to the greatest heights at which material can be detected. In fact, Showalter et al. 2001 noted that the halo's brightness varies as a power-law in z, the vertical distance from the ring plane (Fig. 11.11). The brightness is proportional to $z^{-0.6}$ closest to the ring plane, but steepens to $z^{-1.5}$ a few thousand km away. As a result, most of the halo's material is concentrated within just a few hundred km of the ring plane.

Interestingly, Ockert-Bell et al. 1999 identify a feature that they call "halo bloom" (Fig. 11.6c), which begins further out in the main ring and expands to a full thickness of ~ 600 km at the main ring's inner boundary. This thickness closely matches that of the halo's core cited above. A plausible interpretation is that the bloom and halo core are both composed of fine dust scattered by electromagnetic perturbations but not having yet encountered either resonance. Alternatively, the bloom might arise from kicks in eccentricity that are induced as particles cross the 3:2 Lorentz resonance. This halo bloom may also contribute to the discrepant thickness measurements of the main ring described in the middle of the previous section.
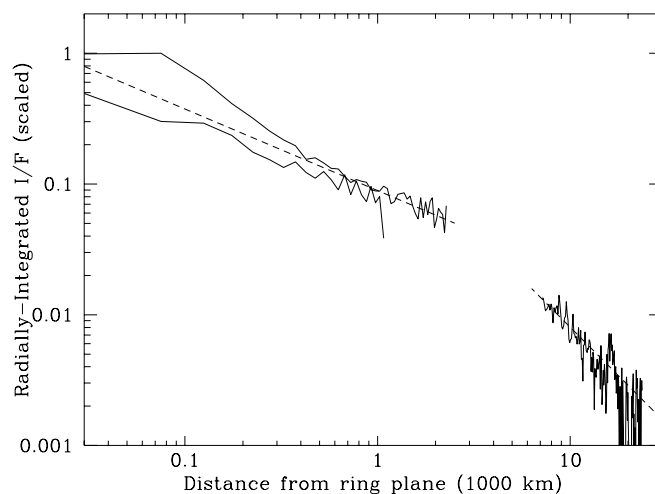
Photometric modeling of the halo is especially challenging because of its diffuse three-dimensional nature, which complicates any comparison of brightness measurements having different viewing geometries. The halo was detected by Voyager and Galileo in forward-scattered light. Unfortunately, the halo has not yet been discerned in Cassini images due to extensive scattered light from the planet. In backscattered light the halo has been sighted from the ground by de Pater et al. 1999, and from HST by Meier et al. 1999 and Showalter (private communication, 2003). Using the 10-m Keck Telescope and working in the 2.2 μm methane absorption band where the planet is especially dark, the halo is revealed. De Pater et al. applied an "onion-peeling" technique to derive the halo's cross-section, finding its form, if not its magnitude, to be reminiscent of the shape of the forward-scattered signal obtained by Galileo. This result is consistent with the expectation that the halo is composed exclusively of dust, because no known perturbation is capable of jostling larger bodies thousands of kilometers out of the ring plane. The Keck data suggest that the halo may be somewhat thinner at this longer wavelength (and in backscatter), perhaps indicating that larger dust is confined more closely to the ring plane. However, this suggestion has not been interpreted quantitatively. The analysis to date is unable to place serious restrictions on the halo's size distribution, al-
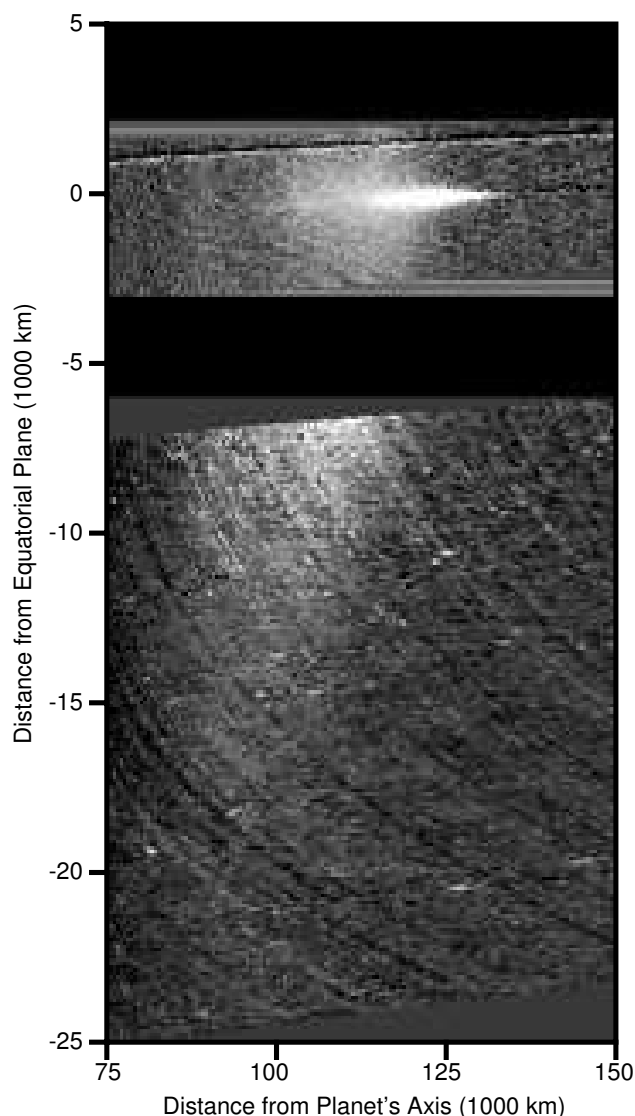
Figure 11.10. Cross-sectional "slices" of two different vertical regions of the halo have been derived from Galileo images 368992300 (upper) and 368976000 (lower). Showalter et al. 1987 describe the image-processing technique employed to develop this figure. We see material that is sharply concentrated near the ring plane (the bright horizontal band at the top of the figure at 0 km elevation) but that spreads more than 20,000 km downwards. Because the images of the two regions have different ranges of phase angles (178.5° vs. 177.3°, respectively) where the brightness changes rapidly with phase, their relative brightness cannot be ascertained. From Showalter et al. 2001.
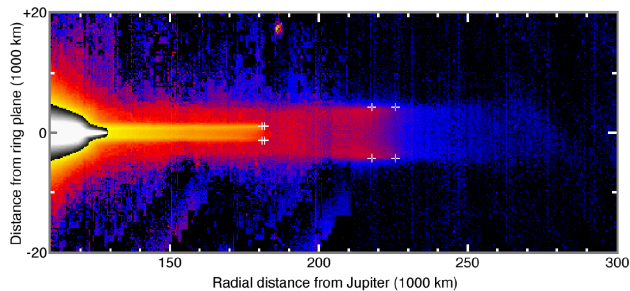

Figure 11.11. The halo's radially integrated intensity is shown as a function of distance from the ring plane, as derived from Fig. 11.10. The data are fit by two straight lines on this log-log plot, indicating a pair of power-law relations, indicating that the slope steepens beyond a few thousand km from the ring plane. From Showalter et al. 2001.

those in the main ring, the halo's normal optical depth is a factor of a few less than that of the main ring. This near-agreement is consistent with the idea that dust is evolving inward continuously from the main ring. According to this model, the overall transition from the flat main ring to the halo is not due to any change in physical properties, but is simply the dynamical consequence of electromagnetic forces (see below). In all other regards, the main ring and the halo are a single tapestry, woven from the same cloth.

11.3.3   Gossamer Rings

The "gossamer rings," the faintest component of the Jovian ring system (see Fig. 11.1), were initially revealed (Showalter et al. 1985) in a lone Voyager image, at a level about 30 times dimmer than the (already faint) main ring. They were interpreted as a flat ring, extending outward perhaps to Thebe's orbit.

It took Galileo's more intensive scrutiny to reveal this ring's true form (Fig. 11.12). It is actually a pair of thick rings, one bounded by the orbit of Amalthea and the other mostly within Thebe's orbit (Ockert-Bell et al. 1999, Burns et al. 1999). In the figure, small plus-symbols mark the radial and vertical limits of each moon's eccentric, inclined orbit. Clearly, there is a very close match between the moons' motions and the rings' thicknesses. Burns et al. describe how dust grains, ejected from the surfaces of each moon, would rapidly disperse in longitude and node (defined as the angle at which a particle's orbit plane crosses Jupiter's equatorial plane) while maintaining their initial inclinations. As such material evolves inward, it would naturally produce the two overlapping, wedge-shaped rings observed. Further support for this interpretation comes from the fact that both gossamer rings show concentrations at the vertical extremes

though the brightening toward high phase and its color less red than the main ring (Meier et al. 1999, de Pater et al. 1999) both imply that dust comprises its major constituent. Reflected light signals returned to HST and Keck during the 2003 ring-plane crossing should allow this conclusion to be tested further.

Showalter et al. 1987 were able to estimate the halo's vertically integrated intensity by suitably co-adding pixels in the Voyager images. Assuming that the dust sizes match

Figure 11.12. This mosaic of four Galileo images (416088922-416089045), taken through the clear filter (0.611 μm) at an elevation of 0.15°, shows the edge-on *gossamer rings* of Jupiter across phase angles of 177-179°. The halo and main ring are over-exposed (solid white with a black outline; cf. Fig. 11.6) at left. White crosses mark the extremes of the radial and vertical motions of Amalthea and Thebe as caused by their eccentric and inclined orbits (Table 1). Clearly Amalthea (whose position is roughly in mid-image) bounds one gossamer ring (its ring is the narrower and brighter strip extending to the right from the main ring); Thebe's ring is the thicker and fainter band reaching yet further right. A very faint outward extension to the Thebe ring is also apparent. This image has been enhanced logarithmically to show all the ring components; in reality the Amalthea ring is approximately ten times fainter than the main ring, while the Thebe ring is ten times fainter again than the Amalthea ring. Note that each gossamer ring is densest along its vertical extremes, particularly the top strip of Amalthea's ring. The image, with a re-projected radial resolution of 400 km, has been expanded vertically by a factor of two to better show the rings' vertical structure. From Burns et al. 2001.

(Fig. 11.12), where particles on inclined orbits spend most of their time.

One component that violates this simple interpretation is an outward extension to the Thebe ring (Fig. 11.12), which is about ten times fainter than the Thebe ring itself. Because it has the same vertical thickness as the Thebe ring, it is likely to be related. In Sec. 11.5.2 we discuss how some material might be found outward of Thebe while the majority of the material evolves inward.

The integrated brightness of each gossamer ring in Fig. 11.12 appears to vary uniformly with distance from Jupiter, although the ring's brightness drops abruptly in Thebe's locale (this is clearly visible in Fig. 15 of Ockert-Bell et al. 1999, which plots the average intensity of the gossamer rings). Since strong Lorentz resonances exist throughout this region, these observations may constrain the charge-to-mass of ring particles (cf. Burns et al. 1999 and Sec. 11.5.2).

If the gossamer ring's dust is perturbed significantly by electromagnetic forces, then one might anticipate that the numerous Lorentz resonances (discussed in Sec. 11.4.2) in the region would be prominent in the rings' visible structure. This is not observed. In fact, the images contain no evidence for an effect from Jupiter's synchronous orbit at 2.24 R_J (160,225 km). (The subtle "synchronous feature" described by Showalter et al. 1985 was probably a result of their misinterpreting the ring as a thin, equatorial structure.)

As in the case of the halo, photometric modeling of the gossamer rings is problematic because of their diffuse structures and overall faintness. Accordingly, the rings' size distributions are undetermined. These rings have been detected in just one Voyager image, a set of Galileo images, and the Keck ground-based results by de Pater et al. 1999. The gossamer rings have been sought in the Cassini images, so far without success. The 2003 HST and Keck data are being searched for the presence of these signatures. Although the substantial brightening at high phase clearly points to fine dust, no detailed modeling of the few available measurements has yet been performed. Assuming dust sizes like those in the main ring, the Amalthea-gossamer-ring's $\tau \sim 10^{-7}$ and Thebe's is five to ten fainter still (Showalter 1989, Burns et al. 2001).

The outer region of the gossamer rings was penetrated by the Galileo spacecraft during its close flyby of Amalthea in which period a few thousand dust impacts were counted; complete data sets were transmitted for some 90 impacts (Krüger et al. 2003). These measurements will allow the first actual comparison of in-situ measurements with the distribution inferred by inverting optical images; however calibration may be troublesome because the instrument was not tested in the laboratory in the appropriate ranges and because of its deterioration in the Jovian magnetosphere. At the time of writing, the as-yet incomplete analysis suggests that small motes dominate the number density whereas larger grains contribute most of the optical depth; the number of impacts increases as Jupiter is approached as does the fraction of small grains. The particle mass distribution appears to be the same in the Thebe ring as in its faint extension, but to be somewhat steeper in the Amalthea ring. The mean particle size is a few microns.

11.4   PROCESSES ACTING ON CIRCUMPLANETARY DUST

11.4.1   Drags and Lifetimes

The photometric behavior described above mandates that grains (microns to tens of microns in size) are prevalent throughout Jupiter's rings and that they account for much –if not all– of the vertical structure visible in forward-scattered images. Tiny particles are substantially influenced by an array of processes (see Fig. 11.13) that are negligible for larger bodies. For example, very small (< 0.05μm), electrically charged ring motes suffer much larger Lorentz accelerations than gravitational ones. In addition, the orbital evolution of bigger grains is governed by non-gravitational forces. These lead to orbital changes that are relatively rapid (timescales are 10–10^5 yr for a 1-μm grain), although not well constrained (see below). Furthermore, such tiny motes live only briefly (10^3–10^5 yr for a 1-μm grain) owing to sputtering by the surrounding plasma and collisions with gravitationally focussed interplanetary micrometeoroids (Burns et al. 1980, Grün et al. 1984, Burns et al. 2001). These two effects imply that, for Jupiter's rings to be long-lived, the dust must be regenerated continually, presumably coming off both seen and unseen source bodies. Expressions for many of these forces and a discussion of the dynamics of Jovian dust are given in Sec. 10.4.1 of the chapter on Jovian dust streams (specifically see Table 10.2 and Fig. 10.9).
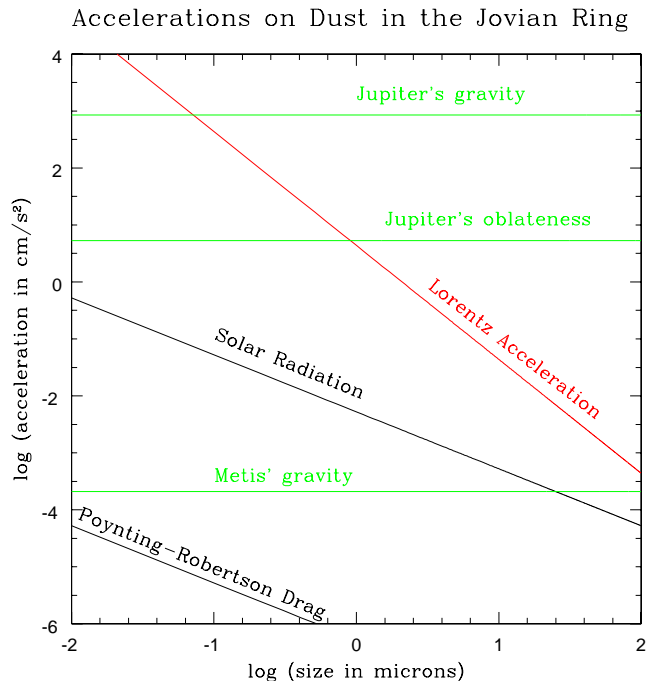
Figure 11.13. Forces on a dust grain (electric potential $= +5$ volts, $Q_{pr} = 1$, $\rho = 2.4$g-cm^{-3}) in the main jovian ring as a function of particle radius. These forces depend on distance a from Jupiter in the following ways: Jupiter's gravity (a^{-2}), Jupiter's oblateness (a^{-4}), Lorentz acceleration (zero at synchronous orbit at $a = 2.24R_J$, then increasing absolutely in either direction away from it; here we plot it for circular orbits at 1.8 R_J), solar radiation pressure (a^0), and Poynting-Robertson drag ($a^{-0.5}$ near Jupiter). Here Metis' gravity (unimportant away from the ring-moon) is estimated for a $\sim$ 1500-km approach to the 20-km satellite. Table 10.2 lists the dependence of these forces on size and distance, while Fig. 10.9 shows the strengths of various perturbations as functions of radial position, albeit exterior to the ring region.

Jovian ring particles develop a significant electric charge (Horányi 1996, Krüger et al., Chapter 10) from the local magnetospheric plasma, ionospheric plasma (Horányi and Cravens 1996) and the photoelectric effect (Horányi and Burns 1991). The calculation of electric charge and several examples are discussed in Sec. 10.4.1 by Krüger et al. who show how charges can vary as a particle enters different ambient environments or as its speed through the plasma is modulated (Burns and Schaffer 1989, Northrop et al. 1989). They argue that, at least for grains in the central magnetosphere, typical electric potentials range from a few volts to tens of volts, with a sign that depends on the local plasma environment and history.

For dust grains in the Jovian system, three main dissipative processes come into play: Poynting-Robertson drag (PR), plasma drag (PD), and so-called "resonant charge variations" (RCV, Burns and Schaffer 1989). Poynting-Robertson drag arises from the momentum transferred when solar photons are scattered and absorbed/re-emitted; it always causes dust grains to lose energy and hence to fall deeper into Jupiter's gravitational well. Plasma drag results from the momentum transferred in both direct physical and indirect Coulomb collisions between a dust grain and the thermal plasma, which moves synchronously with Jupiter's rotating magnetic field; thus, plasma drag causes material to spiral away from synchronous orbit. Finally, RCV takes place when the charge varies periodically as a dust grain's orbit transports it into regions where different plasma conditions dominate or where the grain's speed through the ambient plasma differs; any lag in this charge variation allows the co-rotational electric field to do work, thereby modifying the orbital energy (Burns and Schaffer 1989). Accordingly, depending on the particulars of the charging, RCV can move material *inward* or *outward*. During these drifts, a particle's Jacobi constant (written in the planet's rotating frame) is preserved, meaning that the histories of its a and e are coupled, and RCV cannot push dust grains across synchronous orbit (Hamilton 1994); M. Horányi (private communication, 2003) contends that this prohibition against crossing R_{syn} might no longer be valid when several forces act. Contemporary with the analysis by Burns and Schaffer 1989, RCV was investigated by Northrop et al. 1989, who instead called it "gyrophase drift" since they considered the adiabatic motion of particles with large charge-to-mass ratios. Because both PD and RCV depend strongly on unmeasured properties of the magnetospheric plasma, PR is the sole mechanism whose orbital drift rate is fairly well constrained.

To estimate the relative strengths of these three drag processes (PD, RCV and PR) in the neighborhood of Jupiter's ring, Burns et al. 1999 compared the observed structure of the Jovian ring with the predicted directions of orbital evolution. Exterior to synchronous orbit (located at 2.24 R$_J$), plasma drag produces an outward drift, whereas Jovian ring material is observed to extend primarily Jupiter-ward from the satellites Thebe and Amalthea (Ockert-Bell et al. 1999; see Fig. 11.12). Thus plasma drag is not dominant across the gossamer rings; by inference, it is also not preponderant in the main rings. RCV can produce rapid orbital evolution but has an uncertain sign; since the gossamer rings are uniform in thickness and brightness across the synchronous orbit, where–regardless of sign–this effect changes direction, this evolution mechanism must be relatively weak. By elimination, Poynting-Robertson drag seems to account for the inferred inward drift of Jovian ring particles from their sources. If PR dominates, then the orbital evolution time scale is $\sim 10^5$ r/Q_{pr} yr, where r is measured in microns and Q_{pr} (of order 1 for grains larger than a few microns) is the non-dimensional radiation-pressure coefficient (Burns et al. 1979). On this basis, the grains that are primarily responsible for the ring as seen in forward-scattered light, i.e., those visible in Fig. 11.6, have ages less than a million years.

While this scenario may be plausible, it has one difficulty. Because the predicted sputtering lifetime is much less than this PR age, particles should not survive long enough to be able to evolve across Lorentz resonances. For this reason the PR timescale is not compatible with the primary sources being near the outer edge of Jupiter's main ring. Instead, this argues for widely dispersed suppliers or physical processes that differ from locale to locale or orbital evolution by a process faster than PR (e.g., RCV, Horányi and Cravens 1996). The relative potency of the various processes may, of course, change significantly in various regions; e.g., RCV would be enhanced near Jupiter if a grain's charge in

that vicinity is predominantly set by plasma born in the planet's ionosphere (cf. Horányi and Cravens 1996). This conundrum could possibly be resolved if sputtering ages were lengthened, perhaps because magnetospheric densities in this region were reduced owing to the ring's ability to absorb charged particles (de Pater et al. 1997). However, like in the case of the PR drift times, the sputtering lifetimes seem well-founded since they depend on MeV fluxes measured by Pioneer 11.

An alternative scheme to resolve this puzzle utilizes very rapid inward migration rates (e.g., Horányi and Cravens 1996 consider evolution times of order 10 days), which yield short dynamical lifetimes and an insignificant amount of sputtering and shattering. While nicely avoiding the lifetime problem, this idea leads to inconsistencies of its own. Rapid evolution implies that ring material is lost so quickly from the system that the suppliers themselves may have short lifetimes. While Metis and Adrastea are predicted to survive over the age of the Solar System, the macroscopic backscattering material in the main ring might not be able to. This model also predicts that the micron-sized collisional ejecta produced in high velocity impact obeys a power law with a very steep index of $q = -5.5$ (Horányi and Cravens 1996) as opposed to values near $q = -3.5$ (see Eq. 3) which are more in line with theoretical expectations and laboratory measurements; the latter, however, are for much larger bodies and may not be relevant to micron grains.

11.4.2   Lorentz Resonances

Resonances, which occur whenever forcing frequencies are commensurate with "natural" frequencies of motion, are fundamental throughout dynamics. In studies of the orbital motions of asteroids, satellites and ring particles (Murray and Dermott 1999), perturbations are usually produced by gravitational interactions whereas natural frequencies are those of the orbit. Since perturbation and orbital frequencies vary with location, resonances in celestial mechanics are situated at specific orbital positions. Owing to their radial extent, ring systems present a continuum of orbital frequencies and, as a consequence, contain innumerable resonances, some stronger than others.

Electromagnetic resonances, dubbed "Lorentz resonances" (Burns et al. 1985), occur wherever the frequencies at which a charged mote senses Jupiter's co-rotating magnetic field (Ch. 24 by Khurana et al.) are nearly commensurate with the grain's orbital frequency. Such resonances may play a crucial role in defining Jupiter's ring halo. The strongest of these resonances, so-called "first-order" ones, happen at those positions where a particle orbiting at n rad/sec undergoes a perturbation that varies with frequency $[A/(A-1)]n$, where A is an integer. For dust in the Jupiter system, assuming the planet to be a point mass, Lorentz resonances are located at

$$R_L = [(A-1)/A]^{2/3} R_{syn} = 2.24[(A-1)/A]^{2/3} R_J \qquad (4)$$

(Fig. 11.14). This expression ignores the slight radial shifts associated with the precise amount of electrical charge, an approximation that is valid for micron-sized dust, but not for submicron grains for which the Lorentz force rivals Jupiter's gravity (Fig. 11.13).

Depending upon the speed and direction at which the
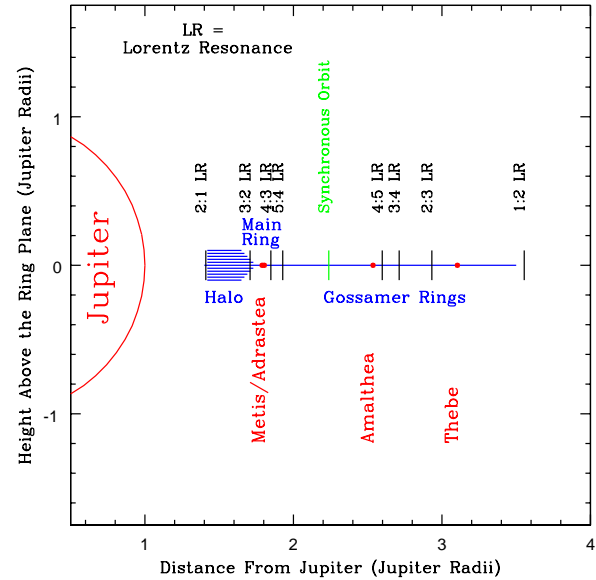
Figure 11.14. Location of some first-order Lorentz resonances in the Jovian system. For orbital drifts that are slow enough, resonant trapping will occur when grains move toward synchronous orbit; resonant jumps in eccentricity and inclination are expected when particles leave the vicinity of synchronous orbit. Note that strong resonances (the 3:2 and the 2:1; i.e., $A = 3$ or 2 in Eq. 4) flank the ring halo and that numerous resonances reside throughout the gossamer rings. The infinite number (Eq. 4 as A gets large, Schaffer and Burns 1987, Hamilton 1994) of ever-weaker resonances that accumulate on R_{syn} are naturally not shown.

grains reach the resonances, their orbits may get trapped there, suffer jumps in a, i and e on passage across the resonance, or slip through largely unscathed (Schaffer and Burns 1987, Schaffer and Burns 1992, Hamilton and Burns 1993, Hamilton 1994). In particular, see Figs. 14 and 15 of Burns et al. 2001, which illustrate the different outcomes that can happen depending on the direction in which a resonance is traversed.

Lorentz resonances, which are claimed above to introduce noticeable features in the halo, lie both exterior and interior to R_{syn}, depending on A's sign. They thus populate the gossamer rings (Fig. 11.14). Despite the expectation that these resonances should affect particle inclinations, no unusual features have been identified in the gossamer rings' thickness. This absence of obvious structures may be caused by eccentricity variations that smear out particle distributions around resonant locations. Additionally, the large inclinations that can be induced may lower line-of-sight optical depths so substantially that the particle densities may simply be below the noise level of the available images (Hamilton et al. 1998); we will return to this point in Sec. 11.5.2. Alternatively, if resonant charge variations dominate (Horányi and Cravens 1996), then radial transport times are rapid and the effects of Lorentz resonances are vitiated.

11.5 THE FORMATION OF JUPITER'S RINGS

This section begins by describing the role of small moonlets as ring-suppliers and then the mechanisms that generate the rings' three structural components: the gossamer rings, the main ring and the toroidal halo.

11.5.1 Ring-moons as Sources

All objects in space are continually bombarded by interplanetary projectiles. Jupiter's ring-moons are particularly so-affected because the collision speeds near Jupiter are many tens of kilometers per second. Because the ring-moons are small bodies, the speeds required for impact ejecta to escape their gravitational grasp, when the satellites are considered isolated spheres, are just tens of m/s. As listed in Table 2, escape is in fact *much* easier from parts of the inner two moons, owing to their elongated shapes, as well as tidal and centrifugal effects (Burns et al. 1999). As recently calculated (P. Thomas, private communication, 2003), Amalthea's low density of ≈ 1 g-cm^{-3} (Anderson et al. 2002) means that material on the long tips of all these satellites is scarcely bound.

Smaller ring-moons may be better sources than larger ones (Burns et al. 1984). As discussed in Sec. 11.5.3, this counter-intuitive result occurs because not all the ejecta from larger targets will be freed if the speeds needed for escape are too high. For this reason Burns et al. 1999 maintain that tiny Adrastea and Metis may supply the main ring more copiously than Thebe and Amalthea do for their gossamer rings.

Both Adrastea and Metis seem to remove material from swaths surrounding their orbits (Figs. 11.6b and 11.7), presumably by forcing trajectories to cross. Burns and Gladman 1998 and Alvarellos et al. 2002 have numerically demonstrated that the half-width of the radial band enveloping a small satellite that is swept clear by satellite interactions is

$$\delta a = 2.4 \ \mu^{1/3} \ a, \tag{5}$$

where μ is the satellite-planet mass ratio; δa is about three times the Hill radius (Murray and Dermott 1999). For the small moons in Jupiter's main ring, we find that $\delta a \sim 4R_{sat}$ if the moon's density is taken to be 1 g-cm^{-3}. Thus Adrastea's clearing zone should be about 70-km wide, while Metis's is two and a half times broader (plotted as vertical bands in Fig. 11.7).

Interior to Adrastea is an enhanced ring density that we take to be caused by grains that have escaped from the smallest visible Jovian ring-moon and then to have drifted inward. However, nothing comparable is visible interior to Metis's path, which implies that smaller Adrastea is the more productive source. We interpret the material exterior to Adrastea (Fig. 11.7) to be large-particle ejecta from collisions onto the satellite whose orbits were boosted to that distance and that have not yet evolved back across Adrastea's path.

11.5.2 Generation of the Gossamer Rings

The innermost gossamer ring extends towards Jupiter from Amalthea, with a vertical thickness that matches the excursions of the satellite above and below Jupiter's equatorial
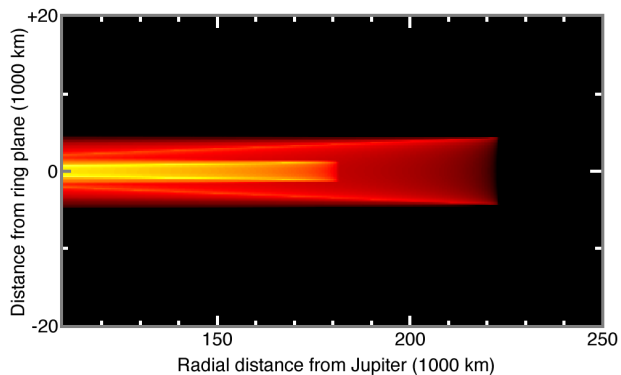

Figure 11.15. A model showing the distribution of material that is launched from Thebe and Amalthea, and then evolves inward at a constant rate. Compare to Figs. 11.12 and 11.16. Each debris ring is composed of *uncharged* material that is created continually at its source moon (either Thebe or Amalthea) and that decays inward at a uniform rate, always retaining its initial inclination but having randomized nodes. The brighter spines that are seen in each debris ring are produced by particles whose orbits have evolved to smaller radii while retaining their initial inclinations. The drift was simply imposed with no particular cause specified. The supply for the Thebe ring is arbitrarily set to be one-half that of the Amalthea ring. From Burns et al. 1999.

plane (Fig. 11.12). Similarly, the grains in the outermost gossamer ring have nearly the same inclinations as the moonlet Thebe.

This one-to-one correspondence between small ring-moons and the outer edges of gossamer rings suggests that the moonlets are the sources of the ring particles which subsequently drift inward. Figures 11.15 and 11.16 graphically test this simple idea. Particles are introduced at the satellite positions and then their orbits are forced to drift uniformly towards Jupiter. As a result of the planet's oblateness, the orbit planes precess rapidly compared to the drift timescale. In Fig. 11.15, the particles are assumed to be uncharged and the model is constructed analytically. Figure 11.16 follows the dynamics of a pair of individual grains (a single emissary from each satellite) under the influences of all of the forces that affect their orbits. Because electromagnetic effects are weak for the large 50-μm grains, the particle in panel A behaves exactly as predicted in the simple analytic model (Fig. 11.15). Some departures from the simple model occur for smaller grains, as illustrated in Fig. 11.16, panel B. Here the Thebe grain is affected by a Lorentz resonance near synchronous orbit ($2.24R_J \approx 161,000$km) while the Amalthea grain is not. The behavior of a dust grain near a resonance depends on the grain size and the drag rate, and is also probabilistic in nature - the particular resonance seen in Fig. 11.16 seems to affect only a small fraction of particles that drift across it (note that none of the grains followed in Fig. 11.17 are significantly affected near $2.24R_J$). Both of these figures should be compared to the Galileo image, Fig. 11.12.

In the image (Fig. 11.12), the upper and lower edges of both the Amalthea and Thebe gossamer rings are seen
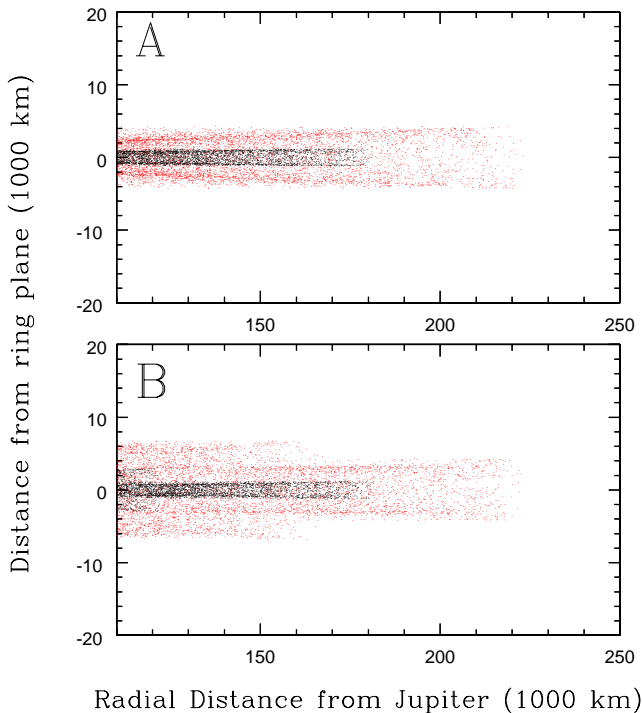
Figure 11.16. Using numerical simulations, the orbits of two $50-\mu$m (Panel A) and 5-μm (Panel B) radius charged dust grains were followed from Amalthea and Thebe as they evolved inward toward Jupiter. The distribution of 50-μm grains is similar to the morphology of the heuristic model (Fig. 11.15) and the Galileo image (Fig. 11.12), indicating that particles of this size are not strongly influences by electromagnetic forces. Smaller dust grains occasionally interact with vertical Lorentz resonances, as this 5-μm Thebe dust grain did near synchronous orbit. These are probabilistic events which depend on both the grain size and the drag rate. A realistic model would combine integrations of numerous particles according to a power-law size distribution. Such a model would predict some "fuzziness" beyond Thebe's maximum excursions from the ring plane; this may or may not be visible in Fig. 11.12. From Burns et al. 1999.

to be brighter than the central strip along the equator. In an epicyclic description of the orbit's vertical motion, particles oscillate sinusoidally across Jupiter's equator plane, so that they reside longer at these extreme vertical locations; this highlights the top and bottom edges of the rings. This phenomenon is apparent in the simulations displayed in Figs. 11.15, 11.16, and 11.17.

These observations of the gossamer rings's structure i) strongly support the contention that the moons are significant sources for the various ring components, and ii) imply that the ring material, once created, evolves inward under a dissipative force (Burns et al. 1999). Inward motion is also consistent with the Jovian halo, which blooms from the ring plane near the location of a strong Lorentz resonance (Burns et al. 1985), which has been demonstrated to excite i during inward drift (Schaffer and Burns 1992, Hamilton 1994, Burns et al. 2001).

One possible inconsistency with this simple picture

is the faint swath of material exterior to Thebe's orbit (Fig. 11.12) since the inclinations of these dust grains implicate Thebe as their source too. Hamilton et al. 1998 and Hamilton et al. 1999 proffer several explanations for this distant material. First, particles evolving inward from Thebe may temporarily reach beyond Thebe's orbit due to eccentricities induced by a strong 2:3 Lorentz resonance located interior to Thebe's orbit (Fig. 11.14). Alternatively, moderate eccentricities might be generated through a different type of resonance, as in Saturn's E ring (Horányi et al. 1992); this would require that the exterior material be negatively charged and has a restricted size centered on a few microns. A third suggestion (M. Horányi, private communication, 2001) is that RCV sorts particles by size, sending some of them inward and thrusting others outward. A final possibility is additional unseen parent object(s) exterior to Thebe supply the ring. This body would need to share the same inclination as Thebe, which seems improbable until one realizes that the same set of Io resonances (Fig. 11.2) that gave Thebe its inclination would impart similar inclinations to any material located between 3.1 and 3.7 R_J (Hamilton et al. 2001).

Perhaps the most striking prediction of the numerical modelling is the extremely diffuse spherical shell of radius 2.9 R_J that encircles Jupiter in Fig. 11.17 (Hamilton 1998). In this simulation, the smaller (1- and 2-μm) grains were captured into the vertical 2:3 Lorentz resonances at 2.9 R_J, which slowly tipped their circular orbits by many tens of degrees. The larger (4- and 8-μm) grains are not captured, and continued inward as in Figs. 11.15 and 11.16. Particles that are trapped at this strong vertical resonance are driven to high inclinations, spreading the particles out so much that they become effectively invisible, perhaps hundreds of times fainter than the already faint gossamer rings. The observational signal for the existence of such a vast shell may have already been seen in the abrupt drop of micron-sized particles detected by Galileo's dust detector (Krüger et al. 2003) as it traversed the gossamer rings between Thebe and Amalthea.

11.5.3   Issues with the Main Ring

The intimate relation of Thebe and Amalthea to their attendant gossamer rings is *prima facie* evidence that small satellites can supply faint rings. Given the location of Adrastea and Metis amidst the outer environs of the main ring, it is thus reasonable to speculate about the role that they play in accounting for the ring's presence. At first glance, the higher density of the main ring compared to that of the gossamer rings seems to contradict the notion that satellites could possibly furnish the main ring's material, since Adrastea and Metis are so small compared to Amalthea and Thebe. We will now argue that, in point of fact, these smaller satellites may be near the ideal size to be sources of ring material. As our discussion of Fig. 11.7 shows, the main ring appears to contain many other parent bodies whose presence is indicated by the ring's back-scattered brightness, and these bodies also contribute significantly.

The rate at which mass, M, is supplied to a ring in time t due to impacts at speed v on an isolated satellite of radius R_{sat} is
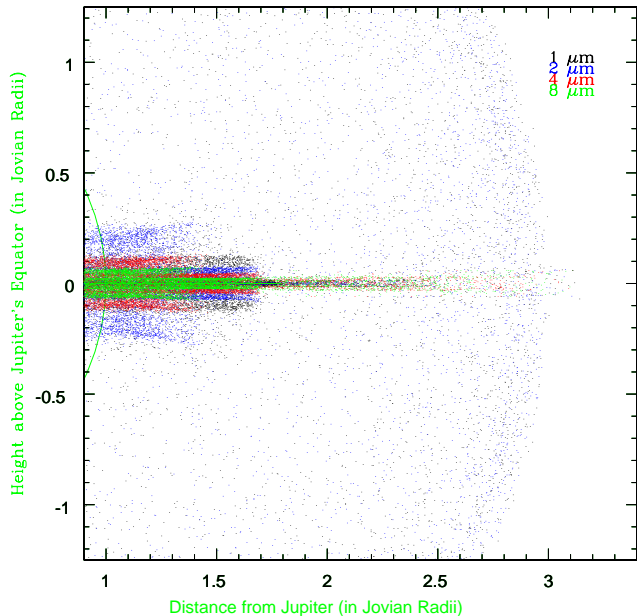
Figure 11.17. The spatial distribution of four different grain sizes (radii of 1, 2, 4, and 8 μm) released from three ring-moons Metis, Amalthea, and Thebe on orbits which are initially like those of the of the parent satellite. Grains from the fourth ring-moon Adrastea behave similarly to those from Metis. The grains evolve under the combined action of gravity, radiation pressure, the Lorentz force (potential = +5 V, particle density ρ = 2.4g-cm^{-3}) and an artificially-enhanced inward drag force. The plot shows where micron-sized grains might be found. Note that no effort is made to correct for the moonlet source strengths or to mimic a realistic power-law size distribution of ring particles. Known features of the jovian ring system seen here are the ring halo (the dense concentration of material between 1.4 and 1.7 R_J) and a combination of the main and gossamer rings (thin horizontal stripe from 1.7 to 3.1 R_J). Hints of the extremely tenuous second inner halo (material inward of 1.4 R_J) are seen in Fig. 11.10. The entire system may be encased in a spherical shell of material $\approx$ 100 times fainter than even the inner halo - this shell may result from inwardly-evolving Thebe dust grains that encounter the 2:3 Lorentz resonance at 2.9R_J (Fig. 11.14). In this simulation, the 1- and 2-μm grains are captured into the 2:3 resonance, but the 4- and 8-μm grains are not. Capture probabilities are a function of both a grain's size and its inward migration speed.

$$dM/dt = \pi \; \phi \; Y \; F_e \; R_{sat}^2, \qquad (6)$$

where ϕ is the mass flux density of hypervelocity impactors, Y is the impact yield (the ratio of ejected mass to projectile mass), and F_e is the fraction of impact ejecta that is moving swiftly enough to escape the satellite (Burns et al. 1984). Y depends on the projectile's specific kinetic energy and is on the order of $10v^2$ for v in units of km-sec^{-1}. ϕ and Y increase close to Jupiter where gravitational focusing causes collisions to be more frequent and more energetic, elevating yields for similar-sized impactors on Adrastea and Metis vs. Amalthea and Thebe. From empirical fits (Greenberg et al. 1978) to hypervelocity-cratering experiments, the fractional

mass ejected above speed $v \sim (v_{crit}/v)^{9/4}$, where v_{crit}, the minimum speed at which impact ejecta is launched, is typically 10 to 100 m-sec^{-1}, depending on the regolith's nature. For an isolated satellite, the escape speed $v_{esc} \propto R_{sat}$. Hence, $F_e \propto R_{sat}^{-1/4}$ if $v_{crit} < v_{esc}$. Thus, counter-intuitively, smaller moons can provide more escaped ejecta than larger moons do. The optimum source has a radius such that its $v_{esc} = v_{crit}$; for a soft regolith and a density of 1 g-cm^{-3}, this radius is 5 to 10 km, like that of Adrastea.

Once ejecta is generated through meteoroid collisions onto Metis and Adrastea, its orbits evolve inward under either PR drag (Burns et al. 1999) or RCV (Horányi and Cravens 1996). The debris starts from the source satellites on nearly circular orbits at roughly 1.8R_J, but the subsequent evolution differs in the two models. If PR drag dominates, inward migration is slow, and particle orbits are ever shrinking circles. If, however, RCV dominates, then evolution is rapid and appreciable orbital eccentricities develop. This difference may be used to discriminate between the two models. The PR drag model predicts a crisp outer edge around Adrastea's orbit at 129,000 km $\approx$ 1.81R_J as seen in Fig. 11.18. If the semimajor axis shrinks under RCV, however, the eccentricity must increase to preserve the particle's electromagnetic Jacobi constant (Horányi and Burns 1991, Hamilton 1994). Accordingly, the maximum apocenter of this material should reach to about 2.0R_J and thus the main Jovian ring would be predicted to extend outward this far. Indeed, this apparently is seen in the RCV model shown in Fig. 11.19, where the planar material extends outward to about 1.95 R_J, with the outer regions composed of short-lived material on highly eccentric orbits. At first sight, this outward extension does not appear to be present in the Voyager and Galileo data (see Figs. 11.6 and 11.7). However, depending on the details of the background subtraction, evidence for this extended "tail" of short-lived grains may be found. Another possibility is that if RCV is combined with strong plasma drag, the brightness of the outward extension would be diminished.

11.5.4 Development of the Halo

Because Saturn's main rings were known to be very thin (as a consequence of energy loss in collisions) all planetary rings were assumed to be similar. Thus the transition of Jupiter's main ring to the vertically extended halo attracted considerable attention immediately following its discovery in the Voyager images. Consolmagno 1980 (see Jewitt 1982 and also Consolmagno 1983) was the first to implicate electromagnetic forces in its explanation. Later Burns et al. 1985 noticed the coincidence between the locations of the transition and the 3:2 Lorentz resonance at 1.71 R_J. Schaffer and Burns (1992) numerically demonstrated that particles drifting through this region would be thrust out of the ring plane as predicted (see Fig. 11.17 and Fig. 11.18). Using the tools of celestial mechanics, Hamilton (1994) advanced the theory further by facilitating the comparison between Lorentz resonances and their better-studied gravitational counterparts. Most recently, Burns et al. (2001) applied these ideas to the new Galileo data (Fig. 11.12).
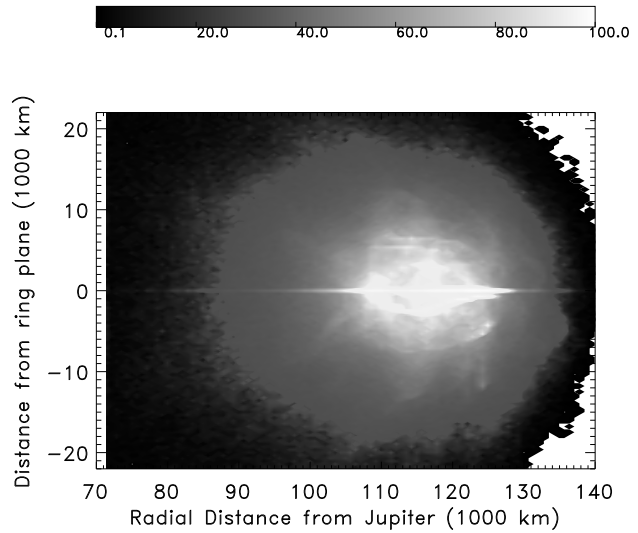
A serious challenge to the Lorentz-resonance picture for the formation of the halo came from Horányi and Cravens (1996), who developed an artificial cross-section of the halo
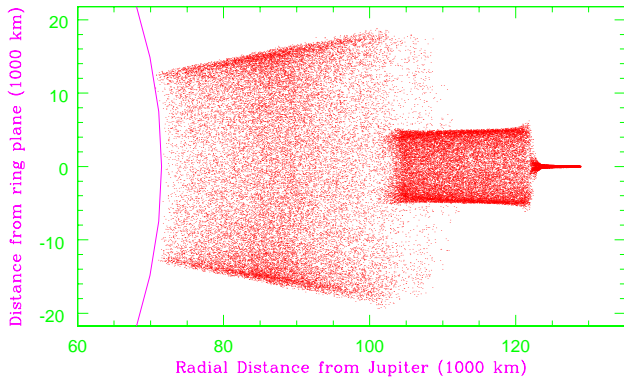
Figure 11.18. A radial cut through the spatial distribution of a 2-μm dust grain released from the Jovian ring-moon Metis (semi-major axis $a = 128,000$ km, or 1.79 R_J) on an initially circular, equatorial orbit. The grain evolves under the combined action of gravity, radiation pressure, the Lorentz force (potential $= +5$ V) and an artificially enhanced drag. The latter permits faster numerical integrations without introducing spurious effects. The drag force pulls the grain in toward Jupiter across the potent 3:2 and 2:1 Lorentz resonances located at 1.71 and 1.41 R_J (see Fig. 11.14), where the grain's inclination and eccentricity receive strong kicks. The thin main ring (between 123,000 km and 129,000 km, or 1.72-1.81 R_J) and the diffuse halo (between 100,000 km and 123,000 km, or 1.40-1.72 R_J) are clearly visible in spacecraft images (cf. Fig. 11.6). The extremely tenuous second "halo" interior to the first has not been definitively identified, although the brightness enhancements inward of 110,000 km and up to 20,000 km from the equatorial plane in Fig. 11.10 are suggestive. From Burns et al. 2001.

Figure 11.19. The number density distribution produced by following 0.5-μm grains in the vicinity of Jupiter's ring. The single size is chosen to best reproduce the halo's structure, and the density of the plot is normalized to 100 at its densest location. All of these grains were started uncharged with a Kepler orbital rate, assuming a uniform surface density of parents through the main ring. Small grains such as these evolve rapidly (typical lifetimes of only 20 days), under RCV, driven by ionospheric plasma, as in the model of Horányi and Cravens 1996. Note the density transition near 128,000km, and the small wing outward, introduced by short-lived grains that have larger eccentricities. From Horányi et al. 2003.

(see Fig. 11.19) by following innumerable particles across this region, arguing that they were driven rapidly inward by resonant charge variations imposed by their charging with ionospheric plasma. The fundamentally new feature of this model is that the effective inward drag rate is up to six orders of magnitude faster than that from Poynting-Roberston drag; lifetimes are estimated as about 100 $(r/\mu m)^3$ days, according to Horányi and Cravens 1996. These same authors (see Horányi et al. 2003) also argue that Jupiter's "contorted magnetic field", rather than Lorentz resonances, led to the high inclinations. This latter point, however, may simply be an issue of semantics. As discussed in Sec. 11.4.2, Lorentz resonances occur at radial locations which, for large grains, are relatively fixed. For small grains, however, the natural radial, vertical, and azimuthal orbital frequencies depart further from the Kepler period, and the locations of the Lorenz resonances shift significantly. Despite their shifts, these resonances remain capable of lofting small grains to large vertical heights. However, other possible mechanisms for exciting the vertical motions of extremely small grains also exist, including the instability discovered by Northrop and Hill (1982). The vertical excursions seen in the Horányi and Cravens model may be due to either or both of these mechanisms, or perhaps even to another as-yet unidentified one.

In addition to making different predictions for the re-

gion of space immediately exterior to the outer edge of the main ring at about 129,000 km or 1.81 R_J, the fast- and slow-drag models also lead to different expectations in the structure of the halo. As seen in Figs. 11.17 and 11.18, slow drag rates lead to halo material between 100,000-120,000km (1.4 and 1.7 R_J) with a vertical extension of $\approx \pm 10,000$km. This is material that has received an inclination kick from the 3:2 Lorentz resonance, but not from the 2:1 resonance (Fig. 11.14). As it crosses 100,000km (the 2:1 Lorentz resonance), material is kicked onto even more highly inclined orbits that further spreads the particle distribution. Some material also attains moderately eccentric orbits and that shortens their dynamical lifetimes. Thus, inward of 100,000km very faint material should be found between $\approx \pm 20,000$km — an even more vertically-extended inner halo.

The fast drag model puts the brightest material in the halo between 105,000 and 125,000km and between $\pm 10,000$km vertically, similar to model just discussed. But fainter material extending up to 20,000 km from the equatorial plane in Fig. 11.19 is predicted to spread between 95,000-130,000km, rather than being confined interior to 100,000km. This is an important observational test that can help distinguish between the two models. Figure 11.10 is the best observational effort to date to detect faint ring material

close to Jupiter and far from the ring plane. The brightest material seems to be confined to about 10,000 km from the ring plane (the classical halo), with fainter material seen only inward of about 110,000 km $\approx 1.5 R_J$, most in line with the inner halo predicted by the slow-drag and Lorentz-resonance model.

11.6 SUMMARY OF JUPITER'S RING-MOON SYSTEM

Jupiter is encircled by a diaphanous ring system (optical depth $\tau \sim 10^{-8} - 10^{-6}$) that extends from ~ 1.3 to > 3.6 R$_J$. Embedded within this ring are four small (radius $R \sim 8$–85 km), irregularly shaped satellites: Metis, Adrastea, Amalthea and Thebe, in order of increasing distance from Jupiter. All components of this system, but for Amalthea, were discovered by Voyager in 1979. This region has been surveyed recently at visible and infrared wavelengths by the Galileo and Cassini spacecraft as well as by ground-based and Earth-orbiting telescopes.

In all giant-planet ring systems, small moons are intimately intermixed amongst the rings, with the satellites acting as both sources and sinks for ring material. At Jupiter these interactions are particularly clear, owing to the quality and quantity of observations, to the lack of optically-thick rings, and to the limited number of small moonlets.

As their craggy overall shapes attest, the small satellites have undergone complex histories of cratering, fragmentation and regolith evolution. Numerous craters separated by ridges dominate their surface morphologies. Crater rims and other topographically high regions are often bright, hinting at down-slope movement. Relatively bright leading hemispheres and blotchy albedo patterns implicate external impactors. Bright features appear to be correlated with crater ridges and raised ridges. The appreciable eccentricities and inclinations of Thebe and Amalthea likely have been induced by resonant interactions occurring during Io's outward tidal migration. Based on a preliminary mass estimate, Amalthea has a low bulk-density (~ 1.0 g-cm^{-3}), implying a rubble-pile interior.

Jupiter's faint dusty rings have three components; from the outside in, these are: i) a pair of very tenuous exterior "gossamer" rings that are derived from the satellites Thebe and Amalthea whose orbits delineate these rings; ii) a 6,500-km-wide, flattened (full-width-at-half-maximum thickness $T < 30 - 100$ km) main ring that exhibits patchiness and through whose outer regions Adrastea skirts; and iii) a radially confined, vertically extended (full width $\sim 20,000 - 40,000$ km), but very equatorially concentrated halo. Except for its outer 1000 km, the main ring's radial and vertical profiles have similar shapes in forward- and back-scattered light, indicating similar radial and vertical placements of large and small particles. In comparison to its reflected-light signal, the main ring is tens to hundreds of times brighter when viewed at visible wavelengths at scattering angles of a few degrees, suggesting that sub-micron- and micron-sized grains produce this highly diffracted signal. The particle size distribution, in the micron range, is $n(r) \sim r^{-2.0 \pm 0.3}$, but it steepens above about 15 μm.

Micron-sized grains have astronomically short lifetimes, implying that the extant particles are being continuously derived from parent bodies. The gossamer rings' unique morphology can be explained by collisional ejecta lost from satellites on inclined orbits. The ejecta evolve inward, apparently under Poynting-Robertson drag. This mechanism may also partially account for the main ring as debris from tiny Adrastea and Metis.

Electromagnetic forces are the primary perturbers of the (small) visible grains; as particles in the main ring drift inward, they cross Lorentz (electromagnetic) resonances at the inner edge of the main ring (at about 1.71 R$_J$), located at the halo's outer edge, and then again near the halo's inner perimeter. Micron-sized particles evolving inward from source bodies in the main ring undergo large inclination jumps at these locations, according to numerical simulations of ring-particle dynamics; in imaging data the ring changes character significantly near these same locales.

11.7 FINAL REMARKS

As we have just summarized, Jupiter's ring-moon complex encompasses many of the topics covered in this book. The planet is central to the system in providing the environment within which the ring-moons and the ring's parent bodies were born and reside. The planet's magnetic field (as well as magnetospheric and ionospheric plasma) influences the orbital evolution of the most visible ring particles. The plasma and meteoroid environments control the physical processes to which the ring components respond, and thereby set the particle lifetimes. The ring-moons are diminutive cousins of the better known major satellites, but a significant history of the complete system's orbital evolution is fossilized in the current orbits of the ring-moons.

Despite its rarified nature, Jupiter's ring system has illuminated our understanding of planetary ring systems because certain effects are highlighted by its low optical depth and by the smallness of its members. In particular it is apparent that modest-size parent bodies populate this ethereal ring system and, through their impact-derived detritus, supply the rings's constituents. The other giant planets also have ring-moons, meaning that they too are undoubtedly cloaked by faint ring systems.

REFERENCES

Acuna, M. H. and N. F. Ness 1976. The main magnetic field of Jupiter. *J. Geophys. Res.* 81, 2917–2922.

Alvarellos, J. L., K. J. Zahnle, A. R. Dobrovolskis and P. Hamill 2002. Orbital evolution of impact ejecta from Ganymede. *Icarus* 160, 108–123.

Anderson, J. D., and 12 colleagues 2002. Gravity field, topography and interior structure of Amalthea. *EOS* December meeting, Abstract P12C-13.

Barbara, J. M. and L. W. Esposito 2002. Moonlet collisions and the effects of tidally modified accretion in Saturn's F ring. *Icarus* 160, 161–171.

Brooks, S. M., L. W. Esposito, M. R. Showalter, and H. B.Throop 2003. The size distribution of Jupiter's main ring from Galileo imaging and spectroscopy. *Icarus*, in press.

Brown, R. H. and the VIMS imaging team 2003. Observations with the visual and infrared mapping spectrometer (VIMS) during Cassini's flyby of Jupiter. *Icarus*, in press.

Burns, J. A. 1986. Some background about satellites. In *Satellites* (J. A. Burns and M. S. Matthews, Eds.), Univ. of Ariz. Press, Tucson, pp. 1–38.

Burns, J. A., and B. J. Gladman 1998. Dynamically depleted zones for Cassini's safe passage beyond Saturn's rings. *Planet. Space Sci.* 46, 1401–1407.

Burns, J. A., and L. E. Schaffer 1989. Orbital evolution of circumplanetary dust by resonant charge variations. *Nature* 337, 340–343.

Burns, J. A., P. L. Lamy, and S. L. Soter 1979. Radiation forces on small particles in the solar system *Icarus* 40, 1–48.

Burns, J. A., M. R. Showalter, J. N. Cuzzi, and J. B. Pollack 1980. Physical processes in Jupiter's ring: Clues for an origin by Jove! *Icarus* 44, 339–360.

Burns, J. A., M. R. Showalter, and G. E. Morfill 1984. The ethereal rings of Jupiter and Saturn. In *Planetary Rings* (R. Greenberg and A. Brahic, Eds.), Univ. of Ariz. Press, Tucson, pp. 200–272.

Burns, J. A., L. E. Schaffer R. J. Greenberg and M. R. Showalter 1985. Lorentz resonances and the structure of the Jovian ring. *Nature* 316, 115–119.

Burns, J. A., M. R. Showalter, D. P. Hamilton, P. D. Nicholson, I. de Pater, and P. C. Thomas 1999. The formation of Jupiter's faint ring. *Science* 284, 1146–1150.

Burns, J. A., D. P. Hamilton and M. R. Showalter 2001. Dusty rings and circumplanetary dust: Observations and simple physics. In *Interplanetary Dust* (E. Grün, B. A. S. Gustafson, S. F. Dermott and H. Fechtig, Eds.), Springer, Berlin, pp. 641–725.

Colwell, J. E., M. Horányi, and E. Grün 1998. Jupiter's exogenic dust ring. *Jnl. Geophys. Res.* 103, 20,023-20,030.

Consolmagno, G. J. 1980. Electromagnetic scattering lifetimes for dust in Jupiter's ring. *Nature* 285, 557–558.

Consolmagno, G. J. 1983. Lorentz forces on the dust in Jupiter's rings. *Jnl. Geophys. Res.* 88, 5607-5612.

Cuzzi, J. N., J. J. Lissauer, L. W. Esposito, J. B. Holberg, E. A. Marouf, G. L. Tyler and A. Boischot 1984. Saturn's rings. In *Planetary Rings* (R. Greenberg and A. Brahic, Eds.), Univ. of Ariz. Press, Tucson, pp. 73-199.

de Pater, I., M. Schulz and S.H. Brecht 1997. Synchrotron evidence for Amalthea's influence on Jupiter's electron radiation belt. *J. Geoph. Res.* 102, No. A10, 22043-22064.

de Pater, I., M. R. Showalter, J. A. Burns, P. D. Nicholson, M. Liu, D. P. Hamilton and J. R. Graham 1999. Keck infrared observations of Jupiter's ring system near Earth's 1997 ring-plane crossing. *Icarus* 138, 214–223.

Dessler, A. (ed.) 1983. *Physics of the Jovian Magnetosphere.* Cambridge U. Press, Cambridge.

Elliot, J., and R. A. Kerr, 1985. *Rings: Discoveries from Galileo to Voyager.* MIT Press, Cambridge.

Esposito, L. W., J. N. Cuzzi, J. B. Holberg, E. A. Marouf, G. L. Tyler, and C. C. Porco 1984. Saturn's rings: Structure, dynamics, and particle properties. In *Saturn* (T. Gehrels and M. S. Matthews, Eds.), Univ. of Ariz. Press, Tucson, pp. 463–545.

Evans, M. W., C. C. Porco, D.P. Hamilton and C.D. Murray 2003. The orbits of the inner jovian satellites Metis and Adrastea. *Astron. J*, submitted.

Fillius, R. W., C. E. McIlwain, and A. Mogro-Campero 1975. Radiation belts of Jupiter: A second look. *Science* 188, 465–467.

Gladman, B. 1993. The dynamics of two close planets. *Icarus* 106, 247–263.

Gradie, J., P. Thomas, and J. Veverka 1980. The surface composition of Amalthea. *Icarus* 44, 373–387.

Gradie, J., S. J. Ostro, P. Thomas, and J. Veverka 1984. Glass on the surface of Io and Amalthea. *J. Noncryst. Solids* 67, 421–432.

Greenberg, R., J. F. Wacker, W. K. Hartmann, and C. R. Chapmen 1978. Planetesimals to planets: Numerical simulations of collisional evolution. *Icarus* 35, 1–26.

Grün, E., G. E. Morfill, and D. A. Mendis 1984. Dust-magnetosphere interactions. In *Planetary Rings* (R. Greenberg and A. Brahic, Eds.), Univ. of Ariz. Press, Tucson, pp. 275–332.

Hamilton, D. P. 1994. A comparison of Lorentz, planetary gravitational, and satellite gravitational resonances. *Icarus* 109, 221–240.

Hamilton, D. P., and J. A. Burns 1993. Lorentz and gravitational resonances on circumplanetary particles. *Adv. Space Res.* 13, #10, 241–248.

Hamilton, D. P., and J. A. Burns 1994. The origin of Saturn's E ring: Self-sustained, naturally. *Science* 264, 550–553.

Hamilton, D. P., J. A. Burns, P.D. Nicholson, M. R. Showalter, and I. de Pater 1998. Do Jupiter's gossamer rings have vertically-extended halos? *BAAS* 30, 1506.

Hamilton, D. P., K. Rauch, and J. A. Burns 1999. Electromagnetic resonances in Jupiter's rings. *BAAS* 31, 1223.

Hamilton, D. P., A. L. Proctor, and K. P. Rauch 2001. An explanation for the high inclinations of Thebe and Amalthea. *BAAS* 33, 1085.

Helfenstein, P., J. Veverka, P. C. Thomas, D. P. Simonelli, P. Lee, K. Klaasen, T. V. Johnson, H. Breneman, J. W. Head, S. Murchie, F. Fanale, M. Robinson, B. Clark, J. Granahan, H. Garbeil, A. S. McEwen, R. L. Kirk, M. Davies, G. Neukum, S. Mottola, R. Wagner, M. Belton, C. Chapman, and C. Pilcher 1994. Galileo photometry of asteroid 951 Gaspra. *Icarus* 107, 37–60.

Horányi, M. 1996. Charged dust dynamics in the solar system. *Ann. Rev. Astron. Astrophys.*, 34, 383–418.

Horányi, M., and J. A. Burns 1991. Charged dust dynamics: Orbital resonance due to planetary shadow. *J. Geophys. Res.* 196, 19283–19289.

Horányi, M., and T. E. Cravens 1996. Structure and dynamics of Jupiter's ring. *Nature* 381, 293–295.

Horányi, M., J. A. Burns, and D. P. Hamilton 1992. The dynamics of Saturn's E-ring particles. *Icarus* 97, 248–259.

Horányi, M., A. Juhasz and T. E. Cravens 2003. Plasma conditions and the structure of the Jovian ring. *J. Geophys. Res.*, to be submitted.

Jewitt, D. C. 1982. The rings of Jupiter. In *Satellites of Jupiter* (D. Morrison, Ed.), Univ. Arizona Press, Tucson, pp. 44–64.

Jewitt, D. C., and G. E. Danielson 1981. The rings of Jupiter. *J. Geophys. Res.* 86, 8691–8697.

Krüger, H., E. Grün, and the Galileo and Ulysses dust science team 2003. Galileo in-situ dust measurements in Jupiter's gossamer ring: First results. Preprint.

McMuldroch, S., S. H. Pilorz, G. E. Danielson, and the NIMS science team 2000. Galileo NIMS near-infrared observations of Jupiter's ring system. *Icarus* 146, 1–11.

Meier, R., B. A. Smith, T. C. Owen, E. E. Becklin, and R. J. Terrile 1999. Near infrared photometry of Jupiter's ring and Amalthea. *Icarus* 141, 253–262.

Mendis, D. A., J. R. Hill, W.-H. Ip, C. K. Goertz, and E. Grün 1984. Electrodynamic processes in the ring system of Saturn. In *Saturn* (T. Gehrels, Ed.), Univ. of Ariz. Press, Tucson, pp. 546–589.

Mishchenko, M. I., and L. D. Travis 1998. Capabilities and limitations of a current FORTRAN implementation of the T-matrix method for randomly oriented, rotationally symmetric scatterers. *J. Quant. Spectrosc. Rad. Transf.* 60, 309–324.

Murray, C.D. and S.F. Dermott 1999. *Solar System Dynamics*, Cambridge U. Press, London.

Nicholson, P. D., and K. Matthews 1991. Near-infrared observations of the Jovian ring and small satellites. *Icarus* 93, 331–346.

Nicholson, P. D., D. P. Hamilton, K. Matthews and C. F. Yoder 1992. New observations of Saturn's co-orbital satellites. *Icarus* 100, 464–484.

Northrop, T.G., and J.R. Hill 1982. Stability of negatively charged dust grains in Saturn's ring plane. *JGR* 87, 6045-6051.

Northrop, T. G., D. A. Mendis, and L. E. Schaffer 1989. Gyrophase drifts and the orbital evolution of dust at Jupiter's gossamer ring. *Icarus* 79, 101–115.

Ockert-Bell, M. E., J. A. Burns, I. J. Daubar, P. C. Thomas, J. Veverka, M. J. S. Belton and K. P. Klaasen 1999. The structure of Jupiter's ring system as revealed by the Galileo imaging experiment. *Icarus* 138, 188–213.

Owen, T., G. E. Danielson, A. F. Cook, C. Hansen, V. L. Hall and T. C. Duxbury 1979. Jupiter's rings. *Nature* 281, 442–446.

Pollack, J. B., and F. Fanale 1982. Origin and evolution of the Jupiter satellite system. In *Satellites of Jupiter* (D. Morrison, Ed.), Univ. Arizona Press, Tucson, pp. 872–910.

Porco, C. C., the Cassini imaging team and 10 colleagues 2003. Cassini imaging of Jupiter's atmosphere, satellites and rings. *Science* 299, 1541-1547.

Schaffer, L. E., and J. A. Burns 1987. The dynamics of weakly charged dust: Motion through Jupiter's gravitational and magnetic fields. *J. Geophys. Res.* 92, 2264–2280.

Schaffer, L. E., and J. A. Burns 1992. Lorentz resonances and the vertical structure of dusty rings: Analytical and numerical results. *Icarus* 96, 65–84.

Showalter, M. R. 1989. Anticipated time variations in (our understanding of) Jupiter's ring system. In *Time-Variable Phenomena in the Jovian System* (Belton, M. J. S., R. A. West, and J. Rahe, Eds.), NASA-SP 494, pp. 116–125.

Showalter, M. R. 1998. Detection of centimeter-sized meteoroid impact events in Saturn's F ring. *Science* 282, 1099-1102.

Showalter, M. R., J. A. Burns, J. N. Cuzzi, and J. B. Pollack 1985. Jupiter's gossamer ring. *Nature* 316, 526–526.

Showalter, M. R., J. A. Burns, J. N. Cuzzi, and J. B. Pollack 1987. Jupiter's ring system: New results on structure and particle properties. *Icarus* 69, 458–498.

Showalter, M. R., J. B. Pollack, M. E. Ockert, L. R. Doyle, and J. B. Dalton 1992. A photometric study of Saturn's F Ring. *Icarus* 100, 394-411.

Showalter, M. R., D. P. Hamilton, J. A. Burns, I. de Pater, and D. P. Simonelli 2001. *Jupiter: Planet, Satellites and Magnetosphere*, Boulder, CO., Abstract booklet, pp. 101-102.

Showalter, M. R., J. A. Burns, I. de Pater, D. P. Hamilton, and M. Horanýi 2001. Recent Hubble Observations of Jupiter's Ring System. em BAAS 35, in press.

Simonelli, D. P., L. Rossier, P. C. Thomas, J. Veverka, J. A. Burns, and M. J. S. Belton 2000. Leading-trailing albedo asymmetries of Thebe, Amalthea, and Metis. *Icarus* 147, 353–365.

Smith, B. A., and the Voyager imaging team 1979a. Jupiter system through the eyes of Voyager 1. *Science* 204, 951–972.

Smith, B. A., and the Voyager imaging team 1979b. The Galilean satellites and Jupiter: Voyager 2 imaging results. *Science* 206, 927–950.

Thomas, P. C., and J. Veverka 1982. Amalthea. In *Satellites of Jupiter* (D. Morrison, Ed.), Univ. Arizona Press, Tucson, pp. 147-173.

Thomas, P., J. Veverka and S. Dermott 1986. Small satellites. In *Satellites* (J. A. Burns and M. S. Matthews, Eds.), Univ. Arizona Press, Tucson, pp. 802–835.

Thomas, P. C., D. Adinolfi, P. Helfenstein, D. Simonelli, and J. Veverka 1996. The surface of Deimos: Contribution of materials and processes to its unique appearance. *Icarus* 123, 536–556.

Thomas, P. C., J. A. Burns, L. Rossier, D. Simonelli, J. Veverka, C. R. Chapman, K. Klaasen, T. V. Johnson, M. J. S. Belton and the Galileo imaging team 1998. The small inner satellites of Jupiter. *Icarus* 135, 360–371.

Throop, H., C. Porco, P. Estrada, P. Helfenstein, L. Dones, R. West, J. Burns, C. Murray, and A. Brahic 2001. Cassini imaging observations of Jupiter's rings. *Jupiter: Planet, Satellites and Magnetosphere*, Boulder, CO., Abstract booklet, p. 115.

Throop, H., C. C. Porco, R. A. West, J. A. Burns, M. R. Showalter and P. D. Nicholson 2003. The jovian rings: New results derived from Cassini, Galileo, Voyager and Earth-based observations. *Icarus*, submitted.

Veverka, J., P. Thomas, P., M. Davies and D. Morrison 1981. Amalthea: Voyager imaging results. *J. Geophys. Res.* 86, 8675–8692.